Liquid Crystals
Publication details, including instructions for authors and subscription information:
http://www.informaworld.com/smpp/title~content=t713926090

Stability of a nematic mesophase with internal degrees of freedom Analysis in terms of catastrophe theory

Vi. K. Pershin[a]; V. A. Konoplev[a]
[a] Ural Polytechnic Institute, Sverdlovsk, U.S.S.R.

To cite this Article Pershin, Vi. K. and Konoplev, V. A.(1992) 'Stability of a nematic mesophase with internal degrees of freedom Analysis in terms of catastrophe theory', Liquid Crystals, 12: 1, 95 — 126
To link to this Article: DOI: 10.1080/02678299208029041
URL: http://dx.doi.org/10.1080/02678299208029041

LIQUID CRYSTALS, 1992, VOL. 12, No. 1, 95–126

Stability of a nematic mesophase with internal degrees of freedom Analysis in terms of catastrophe theory

by Vl. K. PERSHIN* and V. A. KONOPLEV
Ural Polytechnic Institute, 620002 Sverdlovsk K-2, U.S.S.R.

(*Received 15 October 1990; accepted 9 November 1991*)

A model of a nematic mesophase with internal degrees of freedom is developed using the variational principle by means of catastrophe theory methods. It is shown that the free energy of the model being a function of two order and three control parameters is represented in the form of the superposition of local potentials corresponding to elementary fold and swallow tail catastrophes according to Thom's classification. All of the physical conclusions obtained are a consequence of this result. By means of catastrophe theory a bifurcation set (separatrix) of the model is built which divides the control parameters namely the effective molecular length (ε), their rigidity (γ) and the dimensionless temperature (t) of the system space into six non-intersecting parts each parametrizing qualitatively similar potentials. The lower and upper temperature boundaries of the isotropic liquid and orientationally ordered states, respectively, are determined as sub-sets of the bifurcation set in the control parameter space. On the basis of numerical analysis and catastrophe theory the Maxwell set and all the fundamentally different phase diagrams of the model in coordinates 't–γ, t–ε, ε–γ' have been constructed. It is shown that triple and terminal critical points can be realized in the phase diagrams. Physical critical manifolds of the model in variables ε–γ–$\langle P_2 \rangle$ and ε–γ–x are built ($\langle P_2 \rangle$ and x are orientational order and conformational disorder parameters, respectively). Analysis of all of the topologically different phase diagrams of the system has been performed.

1. Introduction

Liquid crystals occupying an intermediate position between crystalline solids and amorphous liquids possess a number of unique physical properties. It is considered [1] that the latter are mainly bound up with orientational ordering of the constituent particles which is the prime characteristic of the mesomorphs. However, molecular models of the mesophases including orientational degrees of freedom describe just a part of the experimental data. Ideas based on the approximation of particles as rigid rods have proved to be of little importance for modelling orientationally ordered systems formed by conformationally flexible molecules (liquid-crystalline polymers, lipids, *n*-alkanes, cyanobiphenyls, truxenes, etc.) and to describe a number of phenomena (the odd-even effect, bounded, induced, reentrant mesomorphism, etc.) taking place in such compounds. Information available up to now [2] concerning the effect of the structure of the mesogenic molecules on the macroscopic properties and thermal stability of mesophases leads to the necessity of accounting for the internal degrees of freedom in theories of liquid crystals [3–11].

Investigation of the mechanism of phase transitions is of particular importance in the field of fundamental problems of polymorphism. In this connection there is always a freedom of choosing some molecular parameters in the model whose physical sense is

* Author for correspondence.

0267–8292/92 $3·00

either not ultimately clear or which vary within rather broad limits. Thus, in the standard situation we give them concrete numerical values and solve a numerical problem by fitting, at best, the theoretical results to the known experimental ones. Of course, such calculations, in themselves, have a certain physical sense. However, for many similar cases we fail to establish whether all of the fundamental, qualitatively different opportunities of the existence of the structural transitions, built into the model, are realized. Because of this, predictive aspects of theoretical calculations are essentially restricted. An adequate analysis can only be fulfilled in terms of catastrophe theory.

Investigation of the peculiarities of smooth functions and parametrized families of such function is the focus of attention of catastrophe theory. Catastrophes themselves are discontinuous changes arising in the form of a sudden response of the system to a continuous alteration of the external conditions. Thom [12] has called such sharp changes catastrophes with the aim of giving the sense of a dramatic alteration of the state of the system at its development. The gradient stationary systems described by families of smooth potentials $\Psi(x, c)$ depending on n state variables (order parameters) $x=(x_1,\ldots,x_n)$ and r control parameters $c=(c_1,\ldots,c_n)$ are the subject of elementary catastrophe theory studies [12–15]. The meaning of the functions $\Psi(x, c)$ is particularly clear in thermodynamics. Establishing the correspondence between the thermodynamic potential and a particular type of catastrophe (see later) allows us, at least locally in the neighbourhood of potential critical points, to use the already known geometric representation of the latter without a detailed analysis. It gives an opportunity to construct phase diagrams of a physical system in limited areas of the control space. Information about the local structure of the solution of the equilibrium equations and that of the phase diagrams is the most valuable for the construction of global phase diagrams since it may be used as initial data for a computer problem *in situ*.

For the family of functions $\{\Psi(x,c)\}$ the majority of points $c=(c_1,\ldots,c_r)$ parametrizes functions possessing non-degenerate (or Morse) points only. For such points the conditions

$$\nabla\Psi(x,c)=0 \quad \det[\partial^2\Psi/\partial x_i\partial y_j]\neq 0, \quad i,\ j=1,\ldots,n$$

are fulfilled. However, the qualitative global behaviour of the family of functions $\Psi(x, c)$ is completely determined by a set of points $c^0=(c_1^0,\ldots,c_r^0)$ which parameterize functions with degenerate critical points. Such a set $\{c^0\}$ of points for which the conditions

$$\nabla\Psi(x,c)=0, \quad \det[\partial^2\Psi/\partial x_i\partial y_j]=0, \quad i,\ j=1,\ldots,n \tag{1}$$

are simultaneously fulfilled is called a bifurcation set or a separatrix of the family of functions $\Psi(x, c)$. The separatrix divides a space $\{c\}$ of control parameters into open areas each of which parametrizes functions $\Psi(x, c)$ of the topologically equivalent (qualitatively similar) type.

In a particular calculation the bifurcation set can be created by proceeding from the system (1) consisting of $(n+1)$ equations and possessing $(n+r)$ unknown quantities $(x_1,\ldots,x_n, c_1,\ldots,c_r)$. Some quantities from the group $c_1,\ldots,c_r$ (their number equals $\min\{r, n+1\}$) should be considered as functions given implicitly by the system (1) and the remainder from the group $(x_1,\ldots x_n, c_1,\ldots,c_r)$ (their number is equal to $[(n+r)-\min\{r,(n+1)\}]$), as independent variables. The result gives a parametric representation of a separatrix.

For physical applications the Maxwell set of a thermodynamic potential is of the greatest interest. This is a set of points in control parameter space for which values of

the potential coincide in two or more isolated critical points (in local minima for physical problems). Discontinuous changes occur in the system when the control parameters change so that the global minimum value of the potential function passes from one minimum to another. These changes have a qualitative character in physical systems only in which the Maxwell rule is valid (for example, it is characteristic for thermodynamic systems including mesophases). From a physical point of view such changes are nothing other than first order phase transitions. It should be noted that qualitative modifications of the potential function type do not occur in this case. Second order phase transitions can take place (but not necessarily) at the bifurcation set only. For their realization the formation of the deepest minimum of the potential is necessary at the bifurcation points. In addition, all of the other minima correspond to metastable states and the potential relief structure changes qualitatively. Thus, establishing the type of the model's bifurcation set and that of the Maxwell set and also of the behaviour of its thermodynamic potential in these sets allows us to determine the nature of phase transitions for the physical system and the topology of the phase diagrams. Note that beyond catastrophe theory limits the construction of all of the fundamentally different phase diagrams of complex multiparametric models is, probably, impossible or causal.

In the present paper the influence of internal degrees of freedom of molecules on the nematic mesophase stability and on successive phase transitions occurring in it is investigated. With the aim of providing a complete qualitative analysis in terms of elementary catastrophe theory (for the number of control parameters $r \leqslant 5$ [12–15]) we proceed from the model hamiltonian of the pseudospin type considered in [16–23] while solving a statistical problem by means of the variation mean field method [24]. Section 2 deals with the description of the model of a mesophase with internal degrees of freedom and with the derivation of equilibrium equations. The main calculation formulae of catastrophes of this model are deduced in §§ 3, 4.1, 4.2 and the Appendices. A bifurcation and Maxwell set of the system are constructed and topological peculiarities of the thermodynamic potential are described in § 4.3. All of the topologically different two dimensional phase diagrams of the model are considered in § 4.4. A numerical analysis of the model is given in §§ 4.5 and 4.6. Correlations of the physical characteristics of the model with the properties of mesogens are discussed in § 5.

2. Description of a model of a mesophase with internal degrees of freedom

To solve the problem just described the dependence of the interparticle interaction on intramolecular changes has to be taken into account. Presuming that together with orientational degrees of freedom the constituent molecules also possess internal (for example, conformational) degrees of freedom we write the hamiltonian for the system in the pseudospin approximation [16–23]

$$H = -\frac{1}{2}\sum_{i,j=1}^{N}\sum_{\alpha,\beta=1}^{\nu}\sum_{k\geqslant 1} V_{\alpha\beta}^{(k)}(ij)P_{2k}(\cos\theta_{ij})n_\alpha(l_i)n_\beta(l_j) + \sum_{j=1}^{N} E(l_j). \tag{2}$$

Here N is the number of particles; $P_{2k}(\cos\theta)$ is the $2k$ order Legendre function; θ_{ij} is the angle between the long axes of the i and j particles; ν is the number of internal (conformational) states of the molecules; quantities $n_\beta(l_i)$ being equal to 1 or 0 describe the presence or absence of the i particle in the β state so that the equality

$$\sum_{\alpha=1}^{\nu} n_\alpha(l_i) = 1 \tag{3}$$

is realized. A certain set of molecular configurations $\{l_i\}$ described by configuration energies $E(l_i)$ corresponds to each conformation [17–19]. Values of the interparticle interaction described by the parameters $V^{(k)}_{\alpha,\beta}(ij)$ depend on that in which α,β conformational states molecules i and j are located. At low temperatures the particles occupy the most ordered conformational states to which a minimum intra- and intermolecular interaction corresponds. Henceforth we consider that conformational rearrangements occur at the level of individual molecules though in this approach we can use a general notion of structural elements without specifying whether it relates to central fragments, flexible parts of molecules, to molecules of a liquid crystal as a whole or to metastable complexes of particles (clusters) [25]. The most important feature of the model is the availability of various internal states in structural elements forming the mesophase which differ through the strength of interaction with a local environment.

To calculate the free energy F of the system we use the variational method [24] according to which

$$F \leqslant F_v = F_0 + \langle H - H_0 \rangle,$$

where

$$F_0 = -kT \ln \mathrm{Tr} \exp(-H_0/kT)$$

is a free energy calculated by means of the trial hamiltonian H_0; F_v is a variational free energy of the system; the brackets $\langle \ldots \rangle$ indicate a thermodynamic average with the hamiltonian

$$H_0 = -\rho \sum_{i=1}^{N} P_2(\cos\theta_i) + \sum_{i=1}^{N} \sum_{\alpha=1}^{v} h_\alpha n_\alpha(l_i) + \sum_{j=1}^{N} E(l_j). \tag{4}$$

Here θ_i is the angle between the long axis of molecule i and the director; ρ, h_β $(\beta = 1,\ldots,v)$ are variational parameters. At the approximation of nearest neighbours $(V^{(k)}_{\alpha\beta}(ij) = V^{(k)}_{\alpha\beta}(ii+r)$, $r = 1,\ldots,\kappa$; κ is their number) and of the uniaxiality of the molecular ordering [1] the variational free energy of one molecule is

$$f_v = -kT \ln \int_0^1 du \exp[\rho P_2(u)/kT] - kT \ln \left[\sum_{\alpha=1}^{v} z_\alpha \exp(-h_\alpha/kT) \right] - \sum_{\alpha=1}^{v} h_\alpha \langle n_\alpha \rangle$$

$$- \frac{1}{2} \sum_{k \geqslant 1} \langle P_{2k} \rangle^2 \sum_{\alpha,\beta=1}^{v} V^{(k)}_{\alpha\beta} \langle n_\alpha \rangle \langle n_\beta \rangle + \rho \langle P_2 \rangle. \tag{5}$$

The orientational order parameters

$$\langle P_{2k} \rangle = \int_0^1 du\, P_{2k}(u) \exp[\rho P_2(u)/kT] \Big/ \int_0^1 du \exp[\rho P_2(u)/kT], \tag{6}$$

characterize the uniaxial order of the constituent particles, and the conformational order parameters

$$\langle n_\alpha \rangle = z_\alpha \exp(-h_\alpha/kT) \Big/ \sum_{\beta=1}^{v} z_\beta \exp(-h_\beta/kT) \tag{7}$$

describe the fraction of molecules in the α conformation; the energetic parameters

$$z_\alpha = \sum_{l_i(n_\alpha(l_i)=1)}^{v} \exp[-E(l_i)/kT], \tag{8}$$

depend weakly on temperature [17–19]; henceforth they are considered as parameters of the problem and are included in equation (5). The condition of a minimum of the variational free energy from equation (5) relative to the variational parameters leads to the equations

$$\left.\begin{aligned} &\rho\partial\langle P_2\rangle/\partial\rho-\kappa\sum_{k\geqslant 1}\langle P_{2k}\rangle\partial\langle P_{2k}\rangle/\partial\rho\sum_{\alpha,\beta=1}^{\nu}V_{\alpha\beta}^{(k)}\langle n_\alpha\rangle\langle n_\beta\rangle=0,\\ &\sum_{\alpha=1}^{\nu}\partial\langle n_\alpha\rangle/\partial h_\varepsilon\left[h_\alpha+\kappa\sum_{k\geqslant 1}\langle P_{2k}\rangle^2\sum_{\beta=1}^{\nu}V_{\alpha\beta}^{(k)}\langle n_\beta\rangle\right]=0,\quad \varepsilon=1,\ldots,\nu;\end{aligned}\right\} \tag{9}$$

which, together with equations (5)–(8), allow us to calculate the dependences of the thermodynamic averages $\langle P_{2k}\rangle$ and $\langle n_\beta\rangle$ on the temperature for given values of the intra- and intermolecular interaction parameters and, hence, to describe the equilibrium state of the nematic mesophase with internal degrees of freedom.

3. Potential of the model

For a qualitative analysis of the model we use an approximation of two conformational states ($\nu=2$) [18–21]. In this case possible configurations of the particles are divided into two sub-sets to each of which the non-folded ($n_2(l_i)=1$) and folded ($n_1(l_i)=1$) conformations are associated as maintaining the geometric anisotropy. Such a simplification is not too crude for relatively short chain molecules, for example, with the number of methylene fragments $n\leqslant 16$–20 and even for long chain molecules with repeating structural units. The latter follows from the known experimental fact [26, 27] that a cooperative interaction exists in groups of 8–10 repeating methylene units which allows us to consider them qualitatively as integral units.

The approximation of two conformational states should also describe, satisfactorily, the cooperative effects of conformational rearrangements occurring in the central aromatic fragments if the molecules contain a relatively small number ($\leqslant 4$) of phenyl groups. In addition, a number of fine phenomena (for example, the odd-even effect) are certainly excluded from consideration.

We take the interrelation between the interparticle interaction parameters to have the form

$$V_{nn}:V_{nf}:V_{ff}=1:\gamma:\gamma^2,\quad (0<\gamma<1), \tag{10}$$

(subscripts n and f in equation (10) correspond to non-folded and folded conformations, respectively) allowing us to proceed to the model which includes two parameters γ, V_{nn} instead of the three $V_{\alpha\beta}$ ($\alpha,\beta=$ n, f). It is seen from equation (10) that the parameter γ distinguishes the interaction of molecules in different conformational states. This distinction can be essential ($\gamma\ll 1$) for flexible molecules and insignificant ($\gamma\leqslant 1$) for rigid molecules. The latter means that the parameter γ has the meaning of the effective rigidity of the particles.

Confining ourselves to the first term ($k=1$) in the expansion of the hamiltonian from equation (2) in the Legendre functions (a model of the Maier–Saupe type [28]) we rewrite the free energy in the dimensionless form

$$\begin{aligned} F_\nu/(N\kappa V_{nn})\equiv\Psi(a,x;\varepsilon,\gamma,t)=&-t\ln J_0(a)+ta(2\langle P_2\rangle+1)/3\\ &+t\ln(1-x)+tR(x,\varepsilon)-1/2\langle P_2\rangle^2Q^2(x,\gamma)\end{aligned} \tag{11}$$

and equations of state from expression (9) in the form

$$\left.\begin{aligned}(2/3)at &= \langle P_2\rangle Q^2(x,\gamma),\\ rR(x,\varepsilon) &= (1-\gamma)\langle P_2\rangle^2 Q(x,\gamma).\end{aligned}\right\} \tag{12}$$

The orientational order parameter

$$\langle P_2\rangle = (3/2)J_1(a)/J_0(a) - 1/2, \tag{13}$$

where

$$J_m(a) = \int_0^1 u^{2m}\exp(au^2)\,du, \quad (m=0,1) \tag{14}$$

are the Maier–Saupt integrals and the conformational disorder parameter

$$x \equiv \langle n_1(l_i)\rangle = z_1/(z_1 + z_2\exp[(h_1-h_2)/kT]) \tag{15}$$

are introduced into equations (11) and (12). The parameter x describes the fraction of molecules in the folded conformation. In equations (11)–(15)

$$t = kT/(\kappa V_{nn}), \quad a = 3\rho/(2kT), \quad Q(x;\gamma) = (1-\gamma)x - 1,$$

$$R(x;\varepsilon) = \ln[x/(1-x)] - \varepsilon, \quad \varepsilon = \ln[z_1/z_2]. \tag{16}$$

Let us note that, according to [17, 18], the parameter ε is from formulae (12) and (16) is a parameter associated with the molecular effective length since it is proportional to the number of methylene fragments.

From the point of view of catastrophe theory [13–15] expression (11) describes a family of potential functions with two state variables a, x and three control parameters ε, γ, t. The critical points of the potential Ψ are defined by the solutions of equations (12); its stability matrix equals

$$[\Psi_{ij}] = \begin{bmatrix} \langle P_2\rangle'[2/3t - \langle P_2\rangle' Q^2] & -2\langle P_2\rangle'\langle P_2\rangle(1-\gamma)Q \\ -2\langle P_2\rangle'\langle P_2\rangle(1-\gamma)Q & t/[x(1-x)] - (1-\gamma)^2\langle P_2\rangle^2 \end{bmatrix}, \tag{17}$$

where $\langle P_2\rangle' = d\langle P_2\rangle/da$. Note that the stability matrix is written in this form because of the equilibrium equations (12). There are no fourfold degenerate critical points obtained for the condition that all the elements of the matrix from expression (17) vanish since the inequalities $Q(x,\gamma)\neq 0, \langle P_2\rangle'\neq 0, \gamma < 1$ are carried out in the model under consideration. It indicates that the stability matrix may possess only one eigenvalue equal to zero whose existence is provided by the zero value of the determinant of the matrix from equation (17)

$$(2/3t - \langle P_2\rangle' Q^2)[t/[x(1-x)] - (1-\gamma)^2\langle P_2\rangle^2] = 4\langle P_2\rangle'\langle P_2\rangle^2(1-\gamma)^2 Q^2 \tag{18}$$

and catastrophes with one variable of the A_p type may only correspond to the potential from equation (11) [12–14]. A bifurcation set of the model is determined by the combined solution of equations (12) and (18).

4. Results

4.1. *Fold catastrophe*

The equations of state from expression (12) give implicit dependences of the orientational order $\langle P_2\rangle$ and conformational disorder x parameters on the dimensionless temperature t and on the molecular parameters ε and γ. The solution

$$a^*=0, \quad (\langle P_2\rangle^*=0), \tag{19}$$

$$x^*=\exp(\varepsilon^*)[1+\exp(\varepsilon^*)] \tag{20}$$

is one of the solutions of equations (12) which corresponds to the orientationally disordered state. The isotropic liquid phase free energy is

$$F_I/(N\kappa V_{nn})=-t\ln(1-x), \tag{21}$$

where at equilibrium the quantity x satisfies equation (20). The phase transition is associated with the long range orientational order loss and is determined by the equality of the potentials (11) and (21) when the conditions (12)–(15) and (19), (20), respectively are fulfilled. At the realization of the equality

$$t^*=(1/5)Q^2(x^*,\gamma^*), \tag{22}$$

the coupling parameters of the model at the point (a^*,x^*), the stability matrix is

$$[\Psi_{ij}]=\begin{bmatrix}0 & 0\\ 0 & 2\lambda'\end{bmatrix}, \tag{23}$$

where

$$\lambda'=(1/2)t^*/[x^*(1-x^*)]. \tag{24}$$

It follows from equations (22)–(24) that the expansion of the potential (11) in a Taylor series in variables (a,x) in the neighbourhood of the point (a^*,x^*) and at fixed parameters ε, γ, t has the form

$$\Psi(a,x;\varepsilon,\gamma,t)=\Psi(a^*,x^*;\varepsilon,\gamma,t)+\alpha'x'+\lambda'x'^2+\beta'a'^2+\sum_{k\geqslant 3}\sum_{\substack{i,j=0\\(i+j)=k}}^{k}a_{ij}x'^ia'^j, \tag{25}$$

where the linear transformation of coordinates $x'=x-x^*$, $a'=a$ is used and the coefficients of the Taylor series (25) up to third order are

$$\left.\begin{aligned}\alpha'&=t\ln[x^*/(\exp(\varepsilon)(1-x^*))],\\ \beta'&=\langle P_2\rangle''_0[1/3t-1/2\langle P_2\rangle'_0Q^2(x^*,\gamma)],\end{aligned}\right\} \tag{26}$$

$$\left.\begin{aligned}a_{03}&=1/3\langle P_2\rangle''_0[2/3t-1/5Q^2(x^*,\gamma)],\\ a_{12}&=-4/225(1-\gamma)Q(x^*,\gamma),\ a_{21}=0,\\ a_{30}&=t(2x^*-1)/[6(x^*)^2(1-x^*)^2].\end{aligned}\right\} \tag{27}$$

In these equations the first $\langle P_2\rangle'$ and the second $\langle P_2\rangle''$ order parameter derivatives over the variable a at the point $a=0$ (according to equation (13)) are $\langle P_2\rangle'_0=2/15$, $\langle P_2\rangle''_0=8/(5\cdot7\cdot9)$. Solving equations (19), (20), (22), (27) we find that coefficients α' and β' in the degenerate critical point $(\varepsilon^*,\gamma^*,t^*)$ are zero and the coefficient

$a_{03} = -(1/9)t^*\langle P_2\rangle_0''$ is non-zero at whatever permissible values of the parameters ε, γ and t. According to catastrophe theory [14] this indicates that there exists such a non-degenerate non-linear smooth transformation of coordinates

$$\left.\begin{aligned} x'' &= x' + \alpha'/(2\lambda') + A_{20}(x')^2 + A_{11}x'a' + A_{02}(a')^2 + \ldots, \\ a'' &\approx -(a_{03})^{1/3}(a' + \Delta/(3a_{03})),\ \Delta = \beta' - \alpha' a_{12}/(2\lambda') \end{aligned}\right\} \tag{28}$$

and such a five dimensional neighbourhood (may be a small one) of the point $(x^*, a^*, \varepsilon^*, \gamma^*, t)$ in which the potential (25) can be given approximately in new variables (28) by the form

$$\Psi(a, x; \varepsilon, \gamma, t) = C_0 + \lambda'' x''^2 + d a''^2 - a''^3, \tag{29}$$

where

$$\left.\begin{aligned} C_0 &= \Psi(a^*, x^*; \varepsilon, \gamma, t) - (\alpha')^2/(4\lambda') + p(s'), \\ p(s') &= \Delta(s')^2 + a_{03}(s')^3, \quad s' = -\Delta/(3a_{03}), \\ \lambda'' &= \lambda' - \alpha' a_{03}/(2\lambda'), \quad d = \Delta(a_{03})^{-2/3}, \end{aligned}\right\} \tag{30}$$

$$\left.\begin{aligned} A^1_{20} &\approx A^0_{20} = a_{30}/(2\lambda'), \quad A^1_{11} \approx A^0_{11} = 0, \\ A^1_{02} &\approx A^0_{02} = a_{12}/(2\lambda'). \end{aligned}\right\} \tag{31}$$

In (31) the superscript 0 corresponds to zeroth order in its expansion in α'. According to [14, 15], formulae for the potential (29) and its coefficients (30) are written in first order of perturbation theory over the small value α' and for the coefficients (31) of the transformation (28) it is fulfilled in the corresponding zeroth approximation without detriment for generality.

It follows from equation (29) that the potential (21) of the model in the neighbourhood of the five dimensional point $(x^*, a^*, \varepsilon^*, \gamma^*, t^*)$ whose coordinates satisfy equations (19), (20), (22) is imagined as a fold catastrophe over the variable a with perturbation of the non-universal type. We note that it follows from catastrophe theory [14] that the approximate potential (29) maintains all of the qualitative features of the initial function (11), at least locally, in the neighbourhood of the point $(x^*, a^*, \varepsilon^*, \gamma^*, t^*)$.

4.2. *Swallowtail catastrophe*

In addition to the trivial solution (19), the system of equations (12) has a non-zero solution describing liquid-crystalline ordering. A separatrix of the model corresponding to the values $a \neq 0 (\langle P_2\rangle \neq 0)$ which satisfy equations (12), (18) has the parametric representation

$$\left.\begin{aligned} \varepsilon(a, x) &= \ln[x/(1-x)] + 2(3)^{1/2} a\langle P_2\rangle/(3U), \\ \gamma(a, x) &= [3^{1/2}(x-1) + U]/(3^{1/2}x + U), \\ t(a, x) &= (3^{1/2}x + U)^2 V \langle P_2\rangle^2 x(1-x)/3, \end{aligned}\right\} \tag{32}$$

$$\left.\begin{aligned} U &= [2aV\langle P_2\rangle x(1-x)]^{1/2} \\ V &= [3a\langle P_2\rangle' + \langle P_2\rangle]/[\langle P_2\rangle - a\langle P_2\rangle'] \end{aligned}\right\} \tag{33}$$

We note that the coordinates of the degenerate critical point (a, x) appear as surface parameters in equations (32) and (33).

Let us choose a point $(\varepsilon^0, \gamma^0, t^0)$ on the separatrix (32) so that the parameters a^0, x^0 corresponding to it would be in accord with the highest among possible catastrophes of the A_p type. For that, according to the algorithm described in [14], we expand function (11) in a Taylor series in the neighbourhood of the point (a^0, x^0) for arbitrary values of the parameters ε, γ, t (i.e. $(\varepsilon, \gamma, t) \neq (\varepsilon^0, \gamma^0, t^0)$)

$$\psi(a, x; \varepsilon, \gamma, t) = \Psi(a^0, x^0; \varepsilon, \gamma, t) + \sum_{k \geqslant 1} \sum_{\substack{i,j=0 \\ (i+j)=k}}^{k} b_{ij} (x')^i (a')^j, \tag{34}$$

where

$$x' = x - x^0, \quad a' = a - a^0. \tag{35}$$

Since there are five unknown quantities including two state variables a^0, x^0 and three parameters ε^0, γ^0, t^0 in the case under consideration then coefficients b_{ij} in expansion (34) are to be calculated, at least, up to fifth order inclusive. They have the form presented in Appendix 1 by equations (A 1)–(A 5).

We calculate the eigenvalues of the stability matrix (16)

$$\lambda_1 = 1/2\{(b_{02} + b_{20}) - [(b_{02} - b_{20})^2 + 4b_{11}^2]^{1/2}\} \tag{36}$$

$$\lambda_2 = 1/2\{(b_{02} + b_{20}) + [(b_{02} - b_{20})^2 + 4b_{11}^2]^{1/2}\} \tag{37}$$

and make a linear non-degenerate non-orthogonal transformation of coordinates

$$\begin{bmatrix} a' \\ x' \end{bmatrix} = \begin{bmatrix} -G & b_{11} \\ b_{11} & G \end{bmatrix} \begin{bmatrix} z_2 \\ z_1 \end{bmatrix}, \tag{38}$$

where

$$G = b_{20} - \lambda_1. \tag{39}$$

In the new variables z_1 and z_2 the mixed second order term in the expansion (34) vanishes and the latter becomes

$$\Psi(a, x; \varepsilon, \gamma, t) = \Psi(a^0, x^0; \varepsilon, \gamma, t) + \beta_{01} z_2 + \alpha z_1 + \delta z_2^2 + \mu z_1^2 + \sum_{k>1} \sum_{\substack{i,j=0 \\ (i+j)=k}}^{k} c_{ij} z_1^i z_2^j. \tag{40}$$

Coefficients in this equation up to fifth order inclusive are presented in Appendix 2 by equations (A 12)–(A 18). It follows from equations (12) and (18) that the eigenvalue from expression (36) and the coefficients $\beta_{01}, \alpha, \delta$ are zero at $(\varepsilon, \gamma, t) = (\varepsilon^0, \gamma^0, t^0)$.

According to [14] in the next step the second highest catastrophe of the model may be established using expressions (A 1)–(A 5), (A 13)–(A 18), (36) and (37) for the coefficients. With this end in view we compose a system of five equations including (12), (18) and two more equations $c_{03} = c_{04} = 0$ (see equations (A 16) and (A 17))

$$\left.\begin{aligned} 2at = 3\langle P_2 \rangle Q^2, \quad tR = \langle P_2 \rangle^2 (1-\gamma) Q, \quad b_{02} b_{20} - b_{11}^2 = 0, \\ -b_{03} b_{20}^3 + b_{12} b_{20}^2 b_{11} - b_{20} b_{21} b_{11}^2 + b_{30} b_{11}^3 = 0, \\ b_{04} b_{20}^4 - b_{13} b_{20}^3 b_{11} + b_{20}^2 b_{22} b_{11}^2 + b_{40} b_{11}^4 = 0. \end{aligned}\right\} \tag{41}$$

A numerical solution of this system using equations (A 1)–(A 11) allows us to find a degenerate critical point

$$\left.\begin{aligned} &a^0 \approx 5{\cdot}8, \quad (\langle P_2 \rangle_0 \approx 0{\cdot}7), \quad x^0 \approx 0{\cdot}77, \\ &\gamma^0 \approx 0{\cdot}56, \qquad \varepsilon^0 \approx 3{\cdot}02, \quad t^0 \approx 0{\cdot}079. \end{aligned}\right\} \tag{42}$$

Substitution of these numerical values into equation (A 18) for coefficient C_{05} using equations (A 1)–(A 11), (36)–(39) shows that

$$b_{05}b_{20}^5 - b_{14}b_{11}b_{20}^4 + b_{23}b_{11}^2b_{20}^3 - b_{50}b_{11}^5|_{(a^0, x^0, \varepsilon^0, \gamma^0, t)} \neq 0, \tag{43}$$

(see formulae (A 18)). According to theorems from [14], the existence of the system's (41) solution (42) for which the inequality (43) is valid indicates that the swallowtail catastrophe is realized for the potential (11) in the neighbourhood of the point $(a^0, x^0, \varepsilon^0, \gamma^0, t^0)$. For the purpose of calculating its explicit analytic representation a non-linear transformation to new coordinates has to be performed

$$z_1' = z_1 + ez_2 + \sum_{k \geqslant 2} \sum_{\substack{i,j=0 \\ (i+j=k)}}^{k} A_{ij} z_1^i z_2^j, \quad z_2' = z_2, \tag{44}$$

in which a precise value of the potential represented by the infinite series (40) may be approximated by its initial part

$$\begin{aligned} \Psi(a, x; \varepsilon, \gamma, t) \approx \Psi(a^0, x^0; \varepsilon^0, \gamma^0, t^0) + \alpha z_1' + \lambda (z_1')^2 \\ + A(z_2') + B(z_2')^2 + F(z_2')^3 + D(z_2')^4 + E(z_2')^5, \end{aligned} \tag{45}$$

containing terms only up to fifth order inclusive. Calculation of the coefficients in this equation is performed in Appendix 3.

Next we introduce the shear transformation

$$z_1'' = z_1' + \alpha/(2\lambda), \quad z_2'' = E^{1/5}(z_2' - S), \tag{46}$$

where

$$S = -D/(5E). \tag{47}$$

Then taking into account this equation, the expression (45) is rewritten using the new variables (46) in the form

$$\Psi(a, x; \varepsilon, \gamma, t) \approx C_0 + \lambda z_1''^2 + cz_2'' + bz_2''^2 - dz_2''^3 + z_2''^5, \tag{48}$$

where

$$\left.\begin{aligned} C_0 &= \Psi(a^0, x^0; \varepsilon, \gamma, t) - \alpha^2/(4\lambda) + P(S), \\ P(S) &= AS + BS^2 + FS^3 + DS^4 + ES^5, \end{aligned}\right\} \tag{49}$$

$$\left.\begin{aligned} c &= E^{-1/5}(A + 2BS + 3FS^2 + 4DS^3 + 5ES^4), \\ b &= E^{-2/5}(B + 3FS + 6DS^2 + 10ES^3), \\ d &= E^{-3/5}(F + 4DS + 10ES^2). \end{aligned}\right\} \tag{50}$$

Hence, it follows from this equation that this model potential is represented by the swallowtail catastrophe relative to the variable z_2'' in the vicinity of the five dimensional point $(a^0, x^0, \varepsilon^0, \gamma^0, t^0)$ whose coordinates (42) satisfy the non-linear equations (41). According to [14], the approximating potential (48) preserves all of the topological peculiarities of the function (11) in the neighbourhood of the point (42).

4.3. *Bifurcation and Maxwell sets of the model*

Using equations (A 1)–(A 22), the equations (20), (21), (24), (27), (29), (30), (36)–(39), (42) and (46)–(50) allow us to calculate the bifurcation and Maxwell sets of this model locally in the vicinity of points $(\varepsilon^*, \gamma^*, t^*)$ and $(\varepsilon^0, \gamma^0, t^0)$ and equations (11)–(15), (18)–(22), (32), (33) and (36)–(40) allow us to do this globally in the whole control parameters space $\{(\varepsilon, \gamma, t)\}$ by use of a numerical analysis. As a result all of the qualitatively different types of the system behaviour at varying thermodynamic and molecular parameters and the complete set of all the possible phase diagrams can be found.

Since the determinant of the stability matrix (23) vanishes on fulfilling the equality (22) then using equation (20) the latter gives the explicit equation for the surface in coordinates (ε, γ, t) being the separatrix of this model's fold catastrophe. The geometry of this separatrix is shown in figure 1 and its physical meaning lies in the description of the dependence of the lowest temperature boundary t^* of the system's isotropic liquid phase absolute stability on the molecular length and flexibility. The geometry of the swallowtail catastrophe separatrix (48) in coordinates (ε, γ, t) is shown in figure 2 (*a*).

The results of numerical calculations of the Maxwell set are shown in figure 2 (*b*). Note that the presentation of two subsets $\{t^*\}$ (see figure 1) and $\{t^B\}$ (see figure 2 (*a*)) of the bifurcation set and Maxwell set $\{t^M\}$ (see figure 2 (*b*)) in different figures is performed for the purposes of visualization only. Projections of two ribs (curves 2 and 6) of the surface $\{t^B\}$ and two ribs (curves 4 and 6) of the surface $\{t^M\}$ onto the plane ε–γ are shown in figure 2 (*c*). Calculation of the Maxwell set was fulfilled by comparison of the minimum values of the local potentials (29) and (48) and by means of that of minimum values of the global potential (11) corresponding to solutions of the systems of equations (12) and (19), (20).

Analysis shows (see figures 1, 2 (*a*) and 3) that separatrix $\{t^*\} U \{t^B\}$ surfaces divide the control parameter space $\{(\varepsilon, \gamma, t)\}$ into six open areas. According to catastrophe theory [14] each of them parametrizes qualitatively similar functions $\Psi(a, x)$ whose topology changes at the separatrix intersection when the control parameters change. In figure 3 qualitative forms of functions Ψ are shown which are parametrized by inner points of the Maxwell set for the section of the space $\{(\varepsilon, \gamma, t)\}$ by the plane

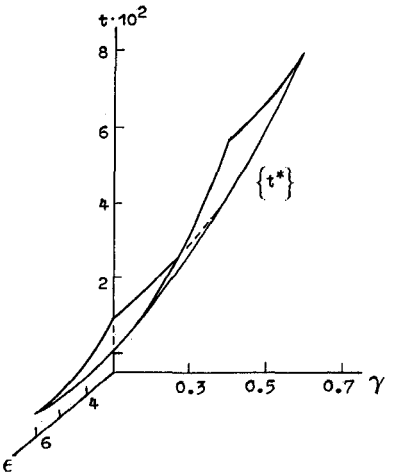

Figure 1. Subset $\{t^*\}$ of the bifurcation set of the fold catastrophe of the model of a nematic mesophase with internal degrees of freedom.

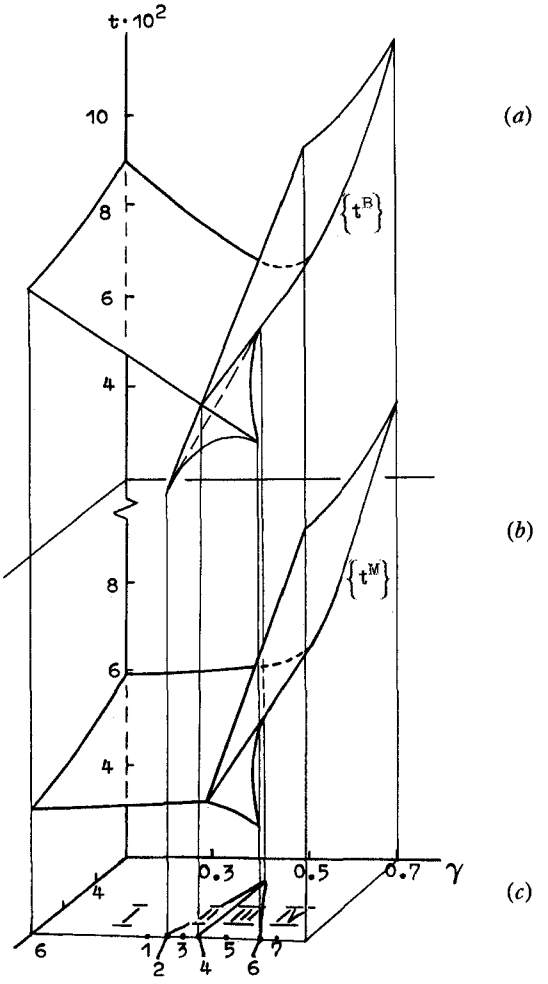

Figure 2. Subset $\{t^B\}$ of the bifurcation set of the swallowtail catastrophe (*a*) and the Maxwell set $\{t^M\}$ (*b*) of the model of a nematic mesophase with internal degrees of freedom. Curves 2, 6 and 4, 6 are projections of the surfaces $\{t^B\}$ and $\{t^M\}$, respectively, on to the ε–γ plane (*c*).

$\varepsilon = \text{const} > \varepsilon^0(\varepsilon = 6)$. Since the topological peculiarities of the free energy of the system is bound up with one variable (a'' in equation (29) and z_2'' in equation (48)) then in these figures and all of the function graphs reflecting a potential topology are, for the sake of visualization only, represented as depending on one variable. The meaning of the latter is, according to equations (28), (38), (44) and (46), close to the orientational order parameter.

The question of phase transformations in the mesophase is solved on the basis of the analysis of the Maxwell set $\{t^M\}$ which is shown in figure 3 by the continuous line. The bifurcation subsets $\{t^B\}$ and $\{t^*\}$ are shown in this figure by dashed and point-dashed lines, respectively. Figure shows also a qualitative shape of the potential Ψ not in points of the Maxwell set (the points and the corresponding graphs 1, 5 8 in figure 3) only but also in points of intersection of the latter with the bifurcation set (the points and the corresponding graphs 2, 4, 6, 7). As we can see from figure 3 at $t = t_{or}$ a phase transition associated with the disruption of long range orientational order is realized in

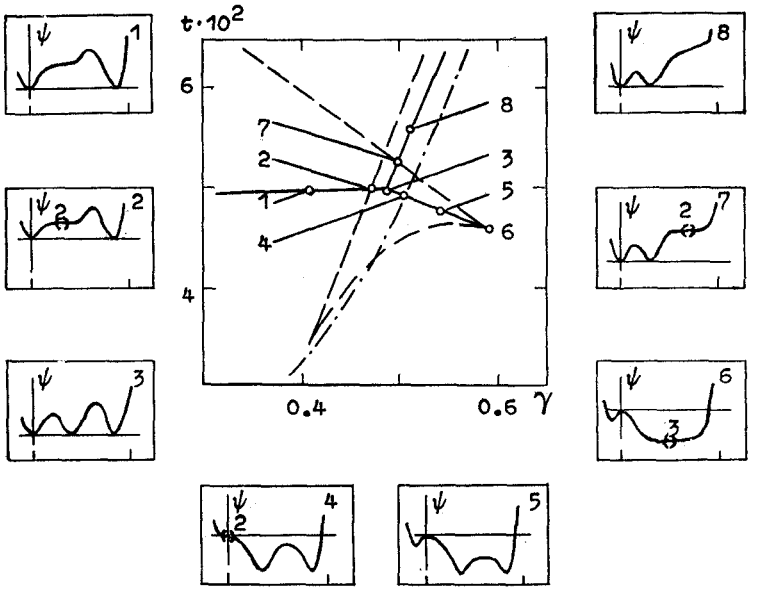

Figure 3. Topology of the free energy of the model (graphs 1–8) in point of the Maxwell set (point 1–8 in the central part of the figure) in the case $\varepsilon = \text{const} > \varepsilon^0$. Broken line in the centre shows the subset $\{t^B\}$, broken line with points, subset $\{t^*\}$ of the bifurcation set; solid line, the Maxwell set $\{t^M\}$.

monotonously decreased section 3–4–5–6 (see the graphs 4, 5, 6) of the $\{t^M\}$ set. The addition, at $t = t_{co}$ an isostructural phase transition between nematic phases with different values of orientational (and conformational) ordering proceeds in its monotonously decreased section 3–4–5–6 (see the graphs 4, 5, 6) of the $\{t^M\}$ set. The phase equilibrium points 2, 4, 7 are simultaneously bifurcation ones in which, besides phase transformations, the degeneracy of the potential Ψ with respect to corresponding metastable states takes place. A common point of three lines of the Maxwell set, the point 3 in figure 3, is a triple point of the system in which at $t = t_{or} = t_{co}$ three different phases (two orientationally ordered and one isotropic liquid) coexist simultaneously (see the graph 3 in figure 3). The point 6 in figure 3 of the t–γ phase diagram is a critical end point in which the difference between low and high temperature partially ordered phases disappears. Note that the critical end point is the only point for the Maxwell set which is simultaneously the one for the bifurcation (i.e. it is a mathematical critical point in which the degeneracy of the potential with respect to thermodynamically stable states takes place).

4.4. *Phase diagrams of the mesophase with internal degrees of freedom*

The bifurcation set $\{t^B\} U \{t^*\}$ and the Maxwell set $\{t^*\}$ whose understanding can be derived from catastrophe theory only allows us to build up all of the topologically different two dimensional phase diagrams of this model and to determine all of the possible paths for the system's evolution from the orientationally ordered state to the disordered state on changing thermodynamic and molecular parameters.

Figures 4 and 5 show the qualitative shapes of the phase diagrams for the system in coordinates t–γ at $\varepsilon = 3 < \varepsilon^0$ and at $\varepsilon = 6 > \varepsilon^0$, respectively. The difference between them is that in the first case, at $t = t_{or}$, an ordinary nematic–isotropic transition is realized and

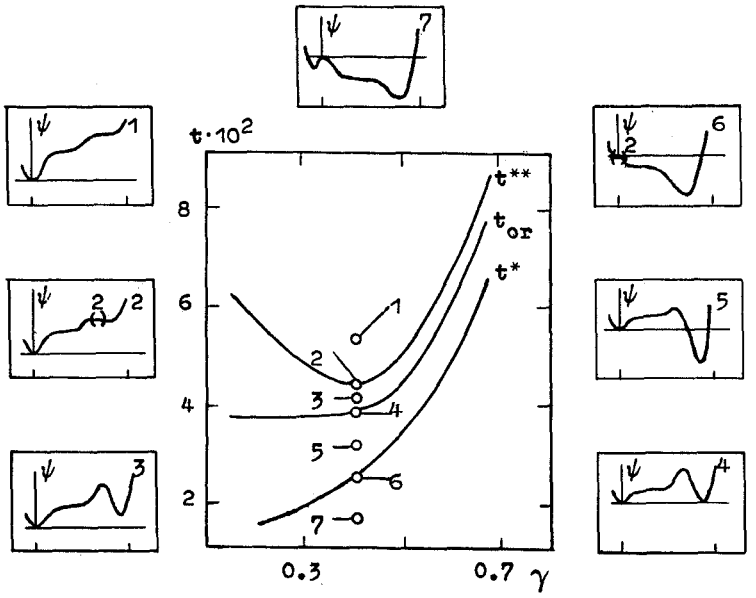

Figure 4. Dependence of the upper temperature boundary t^{**} of the existence of the orientationally ordered state, lowest temperature boundary t^{*} of the existence of the isotropic phase and the temperature t_{or} of the orientational nematic–isotropic transition on the molecular flexibility parameter γ at $\varepsilon = \text{const.} < \varepsilon^0$.

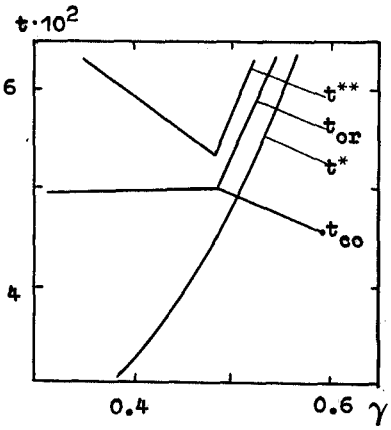

Figure 5. Dependence of the upper temperature boundary t^{**} of the existence of the orientationally ordered state, lowest temperature boundary t^{*} of the existence of the isotropic liquid phase and, respectively, temperature t_{or} of the orientational and t_{co} of the isostructural phase transitions on the molecular flexibility parameter γ at $\varepsilon = \text{const} < \varepsilon^0$.

in the second there is a range of parameters γ for which the system passes through the intermediate state existing in the temperature range $t_{co} < t < t_{or}$ on its way to the liquid state. In addition, dependences of the lowest temperature limit t^{*} of the isotropic liquid stability and of the upper temperature limit t^{**} of the orientationally ordered state stability on the molecular flexibility are shown in figures 4 and 5. We note that the corresponding functions of these figures are topologically equivalent but in the plot $t^{**}(\gamma)$ a sharp minimum is realized at $\varepsilon > \varepsilon^0$ in contrast to a smooth one at $\varepsilon < \varepsilon^0$. The latter is completely stipulated by the swallowtail catastrophe topology (see figure 2 (*a*)).

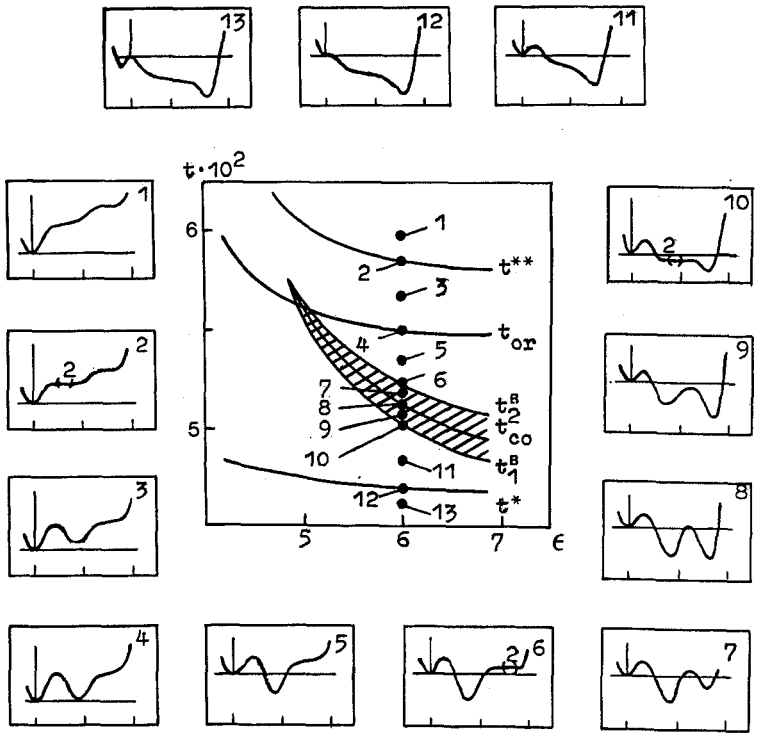

Figure 6. Dependence of the upper temperature boundary t^{**} of the existence of the orientationally ordered state, lower temperature boundary t^{*} of the existence of the isotropic liquid phase, of the temperature of the orientational t_{or} and isostructural t_{co} phase transitions and two temperature branches t_1^B and t_2^B of the bifurcation subset $\{t^B\}$ on the effective molecular length ε at $\gamma = \text{const} \ll \gamma^0$. The area of coexistence of the isostructural nematic phases is hatched.

Figure 6 shows the qualitative shapes of the phase diagrams of the mesophase in coordinates t–ε at $\gamma = 0{\cdot}5 \leqslant \gamma^0$. Corresponding changes in the topology of the potential on decreasing temperature (see the typical points and the graphs 1–13) and dependences of the critical temperatures t^{**}, t^{*}, t_{or}, t_{co} and two branches t_1^B and t_2^B of the bifurcation subset $\{t^B\}$ on the effective molecular length ε are also shown in this figures. It is seen that the mesophase with a lower degree of order competes with the isotropic liquid (graphs 1–5 in figure 6). The partially ordered states compete with each other for the relative stability in the temperature range $t_1^B < t < t_2^B$ (see the graphs 6–10 and the hatched area in figure 6).

4.5. *Temperature evolution of the model*

To analyse the temperature dependence of the mesophase order parameters we consider figure 2 (*c*) where projections of the $\{t^B\}$ and $\{t^M\}$ sets dividing the ε–γ plane into four areas I–IV are shown. Area I where γ is small (and, hence, strong inequalities $V_{nn} \gg V_{nf} \gg V_{ff}$ occur in formula (10)) corresponds to systems of conformationally flexible particles. Area IV where γ is close to 1 and the interaction parameters differ insufficiently in the folded and non-folded conformational states ($V_{nn} \geqslant V_{nf} \geqslant V_{ff}$ in equation (9)) corresponds to systems of conformationally rigid molecules. The intermediate case of semiflexible particles is realized in areas II and III.

The temperature dependence of $\langle P_2 \rangle$ and x corresponding both to inner points of the areas I–IV (points 1, 3, 5, 7 in figure 2(*c*)) and to points located at the boundaries between them (points 2, 4, 6 in figure 2(*c*)) are shown in figures 7–13. Numerical calculations were performed using equations (12)–(16) by considering the sign of the determinant of the matrix (17). The temperature t in figures 7–13 is normalized with the temperature t_{or} of the transition into the isotropic liquid. In figures 7–13 the solid lines correspond to stable states of the system and the thin ones to its metastable, unstable and absolutely unstable states. Their corresponding counterparts are a global minimum, local minima, saddles and local maxima of the free energy surfaces whose reliefs are also shown for characteristic sets of temperature points in these figures.

As we can see from figures 7 and 13, the analogous dynamics of the variation of the free energy is observed in areas I and IV. The free energy, in both cases, have one local minimum at $t \geqslant t^{**}$ (the graphs 6, 7 in figure 7; the graphs 8, 9 in figure 13) and at $t = t^*$ (the graph 2 in figure 7; the graph 4 in figure 13) and two local minima at $t < t^{**}$, $t \neq t^*$ (the graphs 1, 3–5 in figure 7; the graphs 1–3, 5–7 in figure 13). Single valued transitions leading to the loss of long range orientational order are realized in these areas. For the latter ones, however, quantitative differences are observed: in area I a transition into the isotropic phase occurs from the sufficiently more orientationally and conformationally ordered state (see central parts of figures 7 and 13) and at lower temperatures than in area IV (see also figure 3).

Topologically equivalent potentials correspond to points of areas II and III. These potentials have one local minimum at $t \geqslant t^{**}$ (the graphs 10, 11 in figure 9 and the

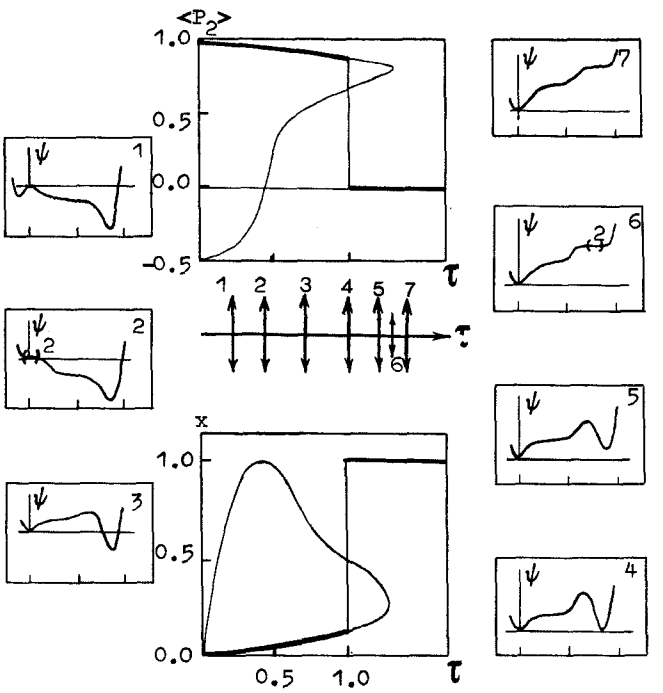

Figure 7. Temperature evolution of our model parametrized by inner points of the area I in figure 2(*c*). Graphs 1–7 show the topology of the free energy in points 1–7 of the temperature axis, central part shows the temperature dependence of the orientational order $\langle P_2 \rangle$ (top) and conformational disorder x (bottom) parameters at $\varepsilon = 6$, $\gamma = 0{\cdot}3$.

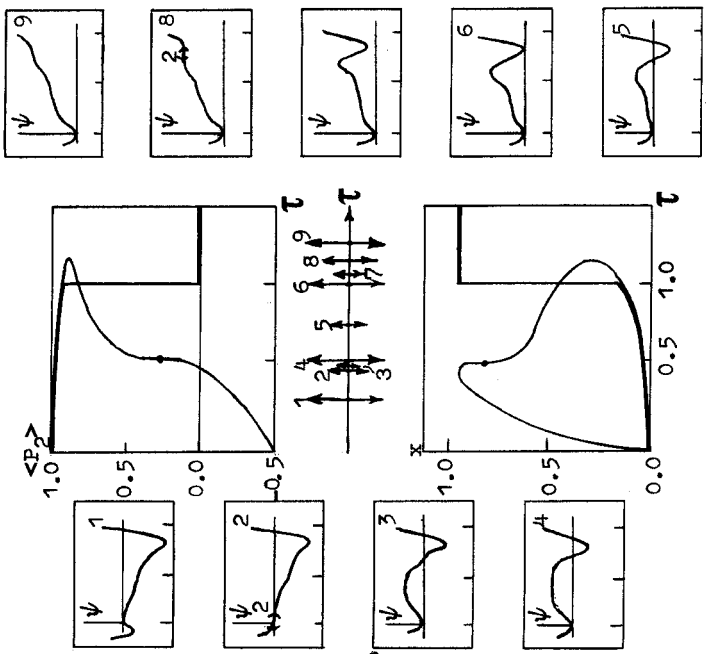

Figure 8. Temperature evolution of the mesophase parametrized by the inner points of the areas I and II in figure 2(*c*). Graphs 1–9 show the topology of the free energy in points 1–9 of the temperature axis, the central part shows the temperature dependence of the orientational order $\langle P_2 \rangle$ (top) and conformational disorder x (bottom) parameters at $\varepsilon = 6$, $\gamma = 0{\cdot}39$.

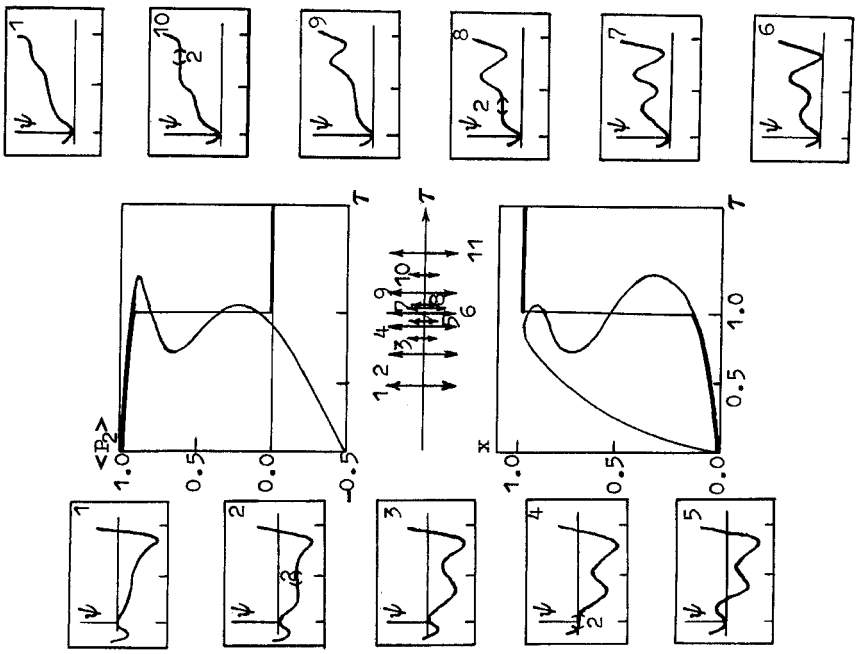

Figure 9. Temperature evolution of the mesophase parametrized by the inner points of the area II in figure 2(*c*). Graphs 1–11 show the topology of the free energy in points 1–11 of the temperature axis, central part shows the temperature dependence of the orientational order $\langle P_2 \rangle$ (top) and conformational disorder x (bottom) parameters at $\varepsilon = 6$, $\gamma = 0{\cdot}42$.

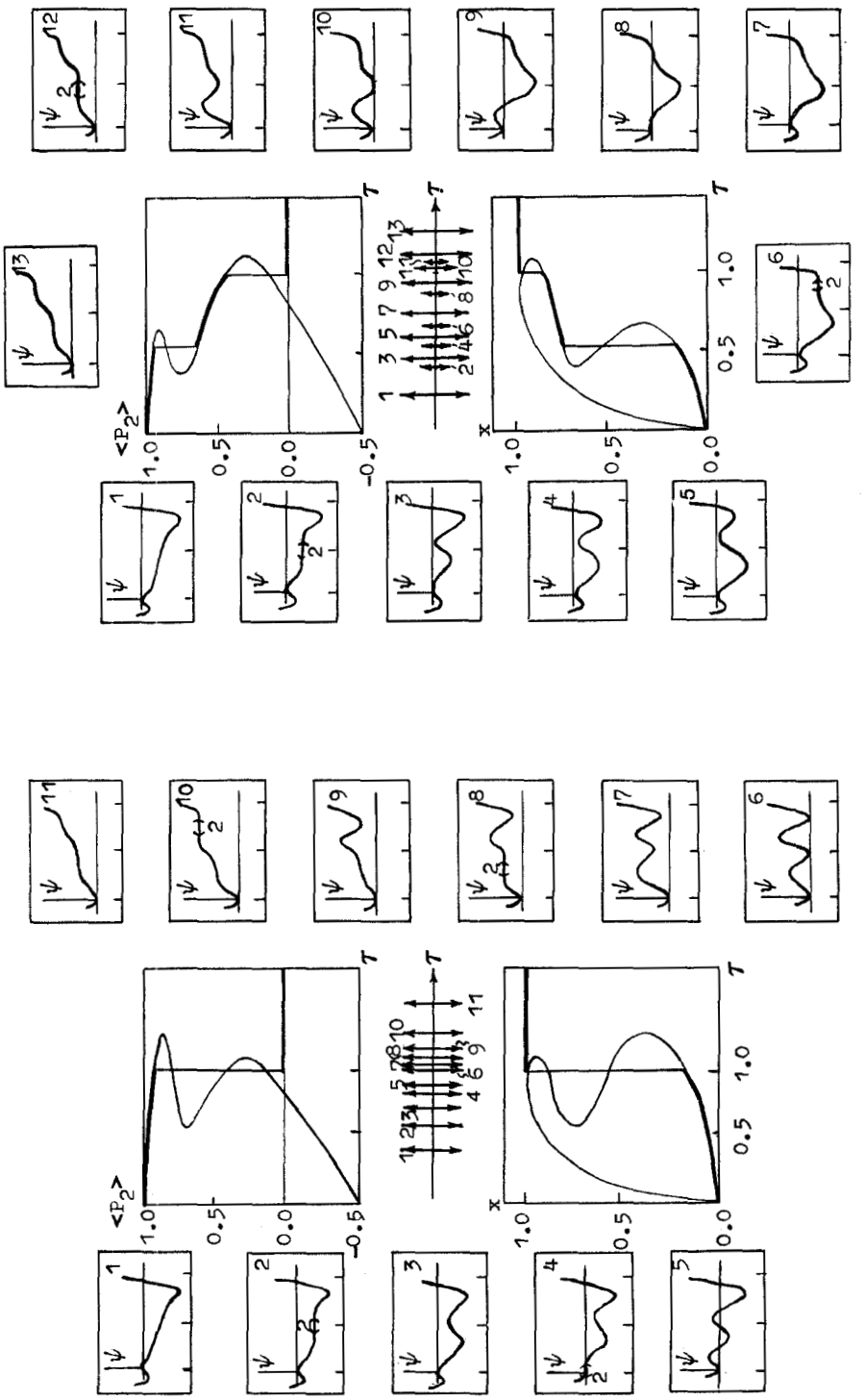

Figure 10. Temperature evolution of the mesophase parametrized by the inner points of the areas II and III in figure 2(c). Graphs 1–11 shows the topology of the free energy in points 1–11 of the temperature axis, the central part shows the temperature dependence of the orientational order $\langle P_2 \rangle$ (top) and conformational disorder x (bottom) parameters at $\varepsilon = 6$, $\gamma = 0{\cdot}47$.

Figure 11. Temperature evolution of the mesophase parametrized by the inner points of the area III in figure 2(c). Graphs 1–13 show the topology of the free energy potential in points 1–13 of the temperature axis, the central part shows the temperature dependence of the orientational order $\langle P_2 \rangle$ (top) and conformational disorder x (bottom) parameters at $\varepsilon = 6$, $\gamma = 0{\cdot}54$.

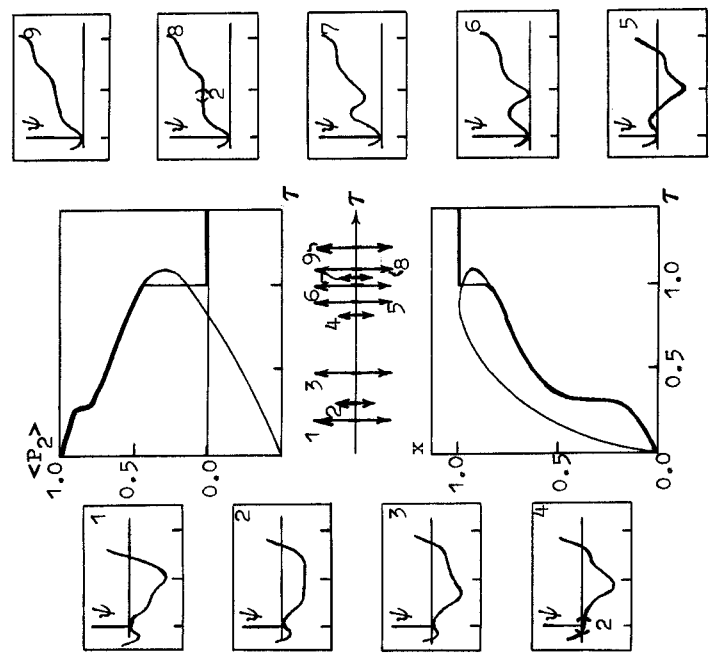

Figure 12. Temperature evolution of the mesophase parametrized by the inner points of the areas III and IV in figure 2(*c*). Graphs 1–9 show the topology of the free energy in points 1–9 of the temperature axis, the central part shows the temperature dependence of the orientational order $\langle P_2 \rangle$ (top) and conformational disorder x (bottom) parameters at $\varepsilon = 6$, $\gamma = 0{\cdot}6$.

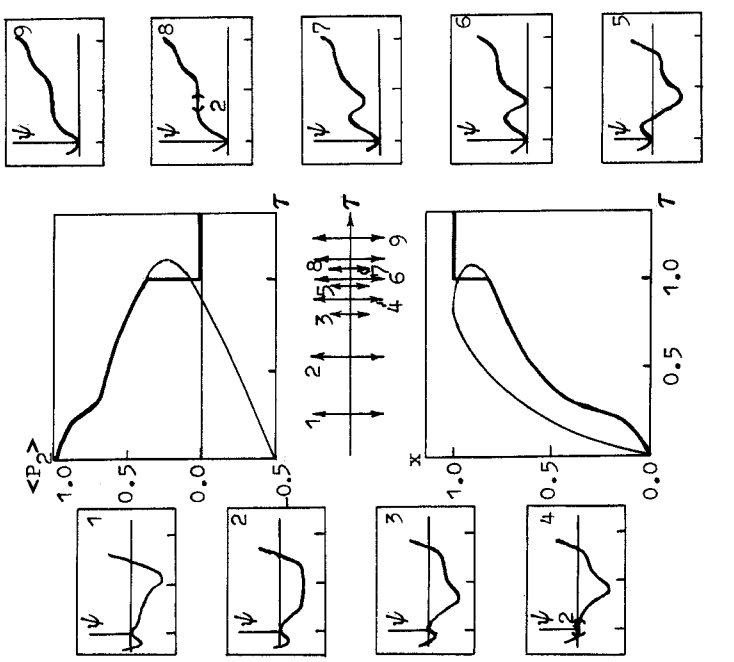

Figure 13. Temperature evolution of the mesophase parametrized by the inner points of the area IV in figure 2(*c*). Graphs 1–9 show the topology of the free energy in points 1–9 of the temperature axis, the central part shows the temperature dependence of the orientational order $\langle P_2 \rangle$ (top) and conformational disorder x (bottom) parameters at $\varepsilon = 6$, $\gamma = 0{\cdot}7$.

graphs 12, 13 in figure 11) and at $t = t^*$ (graph 2 in figure 9 and graph 8 in figure 11), two local minima at $t \leqslant t_1^b, t_2^b \leqslant t < t^{**}$ $(t \neq t^*)$ (graphs 1, 3, 4, 8, 9 in figure 9 and graphs 1, 2, 6, 7, 9–11 in figure 11) or three local minima at $t_1^b < t < t_2^b$ (graphs 5–7 in figure 9 and graphs 3–5 in figure 11). It follows from a comparison of figures 9 and 11 that the main difference of areas II and III is that the partially ordered phase with the greater degree of disorder is metastable in area II and stable in area III.

Figures 8, 10, and 12 show the dependences $\langle P_2 \rangle(t)$ and $x(t)$ (and also free energy reliefs at fixed temperatures) for points of the boundaries between areas I and II, II and III, III and IV, respectively (the points 2, 4, 6 in figure 2 (*c*)). Analysis of these figures is similar to that given previously and so we only note their typical peculiarities. In curves $\langle P_2 \rangle(t)$ and $x(t)$ shown in figures 8 and 12 points of inflection are observed in which the derivatives $d\langle P_2 \rangle/dt$ and dx/dt take infinite values, moreover in figure 12 this occurs in the area of orientationally ordered state. The mathematical nature of these peculiarities follows from the temperature behaviour of the potential (see graphs 1–9 in figures 8 and 12). Thus, the I–II boundary (see figure 2 (*c*)) is a line where the intermediate metastable mesophase occurs; the II–III boundary is a line of triple points in which two liquid-crystalline and one isotropic liquid phase are stable simultaneously; the III–IV boundary is a line of critical points in which the isostructural phase transition between mesophases of similar symmetry but with different degrees of order degenerates into a second order transition.

4.6. *The evolution of ordering on changing the molecular parameters*

Figures 14.1 (*a*) and (*b*) and 14.2 (*a*) and (*b*) show the critical values of $\langle P_2 \rangle$ and x at the phase transition into the isotropic liquid ($\langle P_2 \rangle_{or}$ in figure 14 (*a*) and x_{or} in figure 14 (*b*)) and also critical values of these parameters in isostructural transitions at high order $\langle P_2 \rangle_{c_1}$ in figure 14.2 (*a*) and x_{c_1} in figure 14.2 (*b*)) and at low order ($\langle P_2 \rangle_{c_2}$ in figure 14.2 (*a*) and x_{c_2} in figure 14.2 (*b*)) mesophases depending on the molecular flexibility at fixed values $\varepsilon = \text{const} < \varepsilon^0$ and $\varepsilon = \text{const} > \varepsilon^0$, respectively. Figures 15.1 (*a*) and (*b*) and 15.2 (*a*) and (*b*) show the behaviour of the critical values $\langle P_2 \rangle_{or}$, $\langle P_2 \rangle_{c_1}$ and $\langle P_2 \rangle_{c_2}$ (see figure 15 (*a*) and x_{or}, c_{c_1} and x_{c_2} (see figure 15 (*b*)) depending on the effective molecular length ε at fixed values $\gamma = \text{const} < \gamma^0$ and $\gamma = \text{const} > \gamma^0$, respectively. The calculations were performed using equations (12)–(15) by considering the equality of the energy values (11) and (21) at the minima corresponding to coexisting phases. Note that figures 14 and 15 emphasize a difference in the behaviour of flexible and rigid molecules and also indicate the specific behaviour of semiflexible molecules thus indicating a possibility of realization of discontinuous structural changes conserving the symmetry of the global system.

5. Discussion

The main result of the present paper is a demonstration of the fact that the free energy of our model is represented in the form of the superposition of two local potentials corresponding to fold and swallowtail catastrophes (see equations (6), (9), (11), (29) and (45) and figures 1–3). All of the physical conclusions obtained and discussed later are a consequence of this affirmation.

5.1. *Correlations with properties of individual mesogenic compounds*

Interpretation of the parameters ε and γ as the effective molecular length and flexibility allows us to consider them either as independent or as interconnected quantities. The first case relates to the search for correlations with a model with

properties of individual mesogens. The latter, as we see from § 4.5, can be conventionally divided into four groups in conformity with the four areas of the ε–γ plane in figure 2(*c*). Systems of flexible molecules correspond to the area I; those of molecules with characteristics similar to those inherent in rigid particles correspond to area IV and those of semiflexible molecules for which the formation of intermediate metastable and stable phases is typical correspond to areas II and III, respectively. It has been shown that peculiar types of phase diagrams are inherent to these four classes of molecular systems and specific behaviour of the critical temperatures and values of the orientational order and conformational disorder parameters on changing the length and rigidity of the particles are also characteristic of them (see figures 3–15). Note especially that points in area II in figure 2(*c*) parametrize systems with intermediate phases which do not manifest themselves under ordinary conditions in thermodynamic equilibrium but can be stabilized, for example, in a magnetic field which would change fundamentally the topology of phase diagrams [29]. Areas similar to I, III and IV shown in figure 2(*c*) had been first calculated in [18] but the curvature of the boundaries between corresponding areas is not correctly described there. In addition the area II whose significance becomes apparent from an investigation of systems in external fields [29] and the classification of phase diagrams is not given in [18].

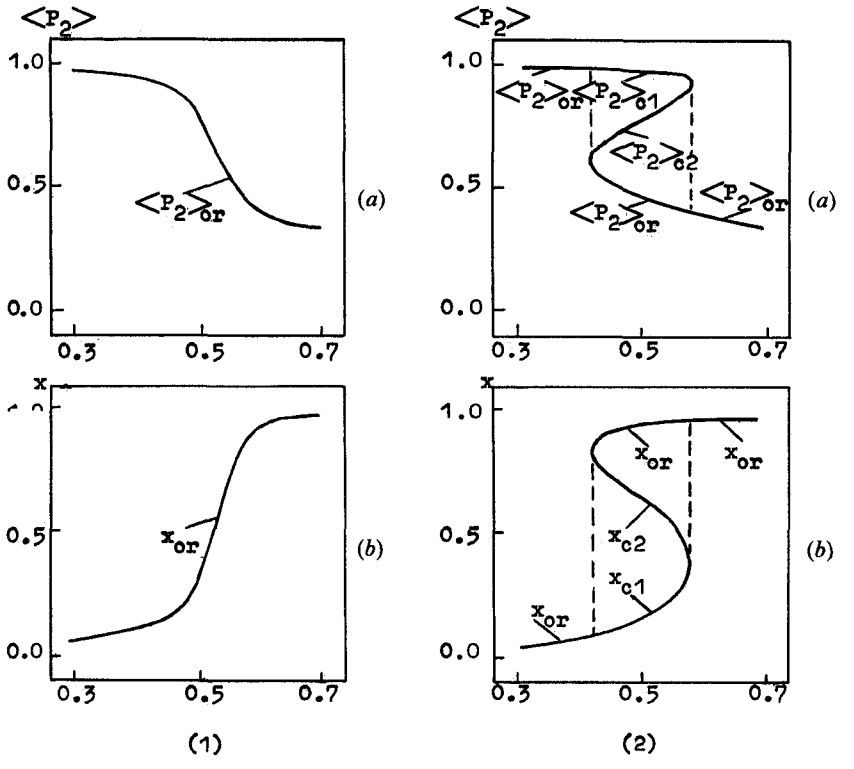

Figure 14. Behaviour of the critical values of the orientational order (*a*) and conformational disorder (*b*) parameters versus the effective flexibility of particles with $\varepsilon < \varepsilon^0(1)$ and $\varepsilon > \varepsilon^0(2)$. $\langle P_2 \rangle_{or}$, x_{or} are jumps of the orientational order and conformational disorder parameters, respectively, at the transition of the mesophase into the isotropic liquid. $\langle P_2 \rangle_{c_1}, x_{c_1}$; $\langle P_2 \rangle_{c_2}$, x_{c_2} are critical values of these parameters at coexistence points of high and low ordered isostructural phases, respectively.

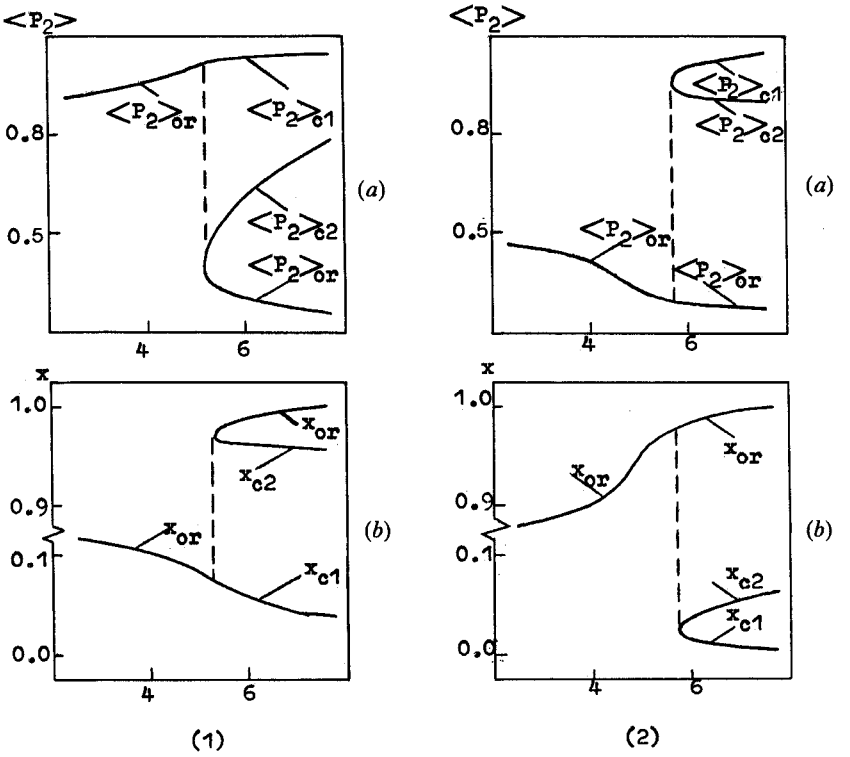

Figure 15. The behaviour of the critical values of the orientational order (*a*) and conformational disorder (*b*) parameters versus the effective molecular length with $\gamma < \gamma^0(1)$ and $\gamma > \gamma^0(2)$. $\langle P_2\rangle_{or}$, x_{or} are jumps of the orientational order and conformational disorder parameters, respectively, at the transition of the mesophase into the isotropic liquid. $\langle P_2\rangle_{c_1}, x_{c_1}, \langle P_2\rangle_{c_2}, x_{c_2}$ are critical values of these parameters at coexistence of high and low ordered isostructural phases, respectively.

A weak change of the orientational order parameter for increasing temperature with its large jump $\langle P_2\rangle_{or}$ at the transition into the orientationally disordered state is characteristic for flexible particles (see figures 7 and 8). Such behaviour is observed in soaps ($\langle P_2\rangle_{or} \approx 0{\cdot}9$ [30]), lecitin ($\langle P_2\rangle_{or} \approx 0{\cdot}7$–$0{\cdot}8$ [31]), long chain linear liquid-crystalline polymers of the aromatic polyesters type ($\langle P_2\rangle_{or} \approx 0{\cdot}6$ [10]), in a number of short chain compounds with terminal ($\langle P_2\rangle_{or} \approx 0{\cdot}7$ [32]) and middle ($\langle P_2\rangle_{or} \approx 0{\cdot}5$ [33]) flexible fragments and has been noted previously in theoretical papers [16–20]. A strong change of the orientational order parameter with increasing temperature with a low jump at the transition into the isotropic liquid is characteristic of rigid particles (see figure 13). Such behaviour has been observed experimentally for many short chain liquid crystals which are well described by the approximation of rigid rods ($\langle P_2\rangle_{or} \approx 0{\cdot}3$–$0{\cdot}4$ [1]) and also in comb-like liquid-crystalline polymers of the polysiloxane type where mesogenic groups which are joined to the main chain by flexible spacers ($\langle P_2\rangle_{or} \approx 0{\cdot}3$–$0{\cdot}4$ [34]) are responsible for the orientational ordering.

It has been shown [35–37] that in homologues of 4-*n*-alklyoxybenzoic acids with $n = 7$, 8, 9 and 10 a specific temperature point is found in the nematic state stability range where a sharp long range orientational order jump occurs which is indicative of the first order phase transition without a change of the global symmetry of the system. According to ideas of authors of papers [36, 37], one of these phases, the high

temperature one, is an ordinary nematic and the other phase, the low temperature one, is a skewed cybotactic nematic. Note that the difference in the intramolecular ordering which manifests itself in the degree of organization of supermolecular order (mesophase cluster formation) can be the basis of the difference between the high and low temperature nematic phases. The supposition is confirmed by X-ray and NMR experiments [38–39] on homologues of aromatic polyesters with an even number of carbon atoms in the spacers which possess a high level of orientational order bound up with specific conformations and which at the same time satisfy the criteria produced for the cybotactic nematic model of short range intramolecular order [26, 27].

Concerning the temperature behaviour of the X-ray scattering intensity, Furuya and Mitsui have found [40] a high temperature phase transition in the liquid-crystalline state of lipid mono and bilayers of pure lecithins and also of their mixtures. The authors of the paper [41] have found that the temperature evolution of these lipid systems proceeds according to the following scheme: a jump in the orientational order parameter from $\langle P_2 \rangle_{c_1} \approx 0{\cdot}7$ to $\langle P_2 \rangle_{c_2} \approx 0{\cdot}3$ takes place at the isostructural transition between liquid-crystalline phases with its following insignificant reduction on increasing temperature and with a second jump into the isotropic liquid which corresponds to the dependence $\langle P_2 \rangle(t)$ shown in figure 11 (cf. figure 10 in [41] and figure 2 (*b*) in [19]). In addition, on the basis of the behaviour of longitudinal and transversal rotational diffusion coefficients a conclusion can be made that at the isostructural transformation a more noticeable conformational disordering jump is observed than at the transition into isotropic liquid. The latter corresponds to what has been shown by the dependence $x(t)$ in figure 11.

5.2. *Critical manifolds and phase diagrams of the model in cylindrical coordinates*

Figures 4–6 and 14–15 show the calculated dependences of the transition temperatures, stability boundaries of the phases and critical values of the order parameters versus the effective rigidity γ and the molecular length ε (cf. figures 3 and 4 in [18]). To compare these results (mostly, at a qualitative level) with the experimental dependences of the analogous physical values on the molecular flexibility found generally from homologous series data it should, necessarily, be taken into account that the values ε and γ are functionally connected. It is clear from physical considerations that increase in the molecular length is to be followed by that of their flexibility and hence, the function $\varepsilon(\gamma)$ should decrease monotonously in the most general situation. Such a functional dependence of ε on γ had been discussed in [18, 19] in which, however, questions fundamental from the point of view of the inner logic of the theory had been left open: should in this case the phase diagrams predicted by the model (see figures 4–6) and the behaviour of critical values (see figures 14 and 15) change? and what type of changes are to be expected?

Beyond the limits of catastrophe theory the solution to this problem consists in recalculating the phase diagrams and critical values dependence of the orientational order and the conformational disorder parameters with specific concrete functions $\varepsilon(\gamma)$. But even in this case it is not perfectly clear that all of the possible, in principle, versions are taken into account. Note that such recalculations were not reported in [18, 19] and it had been implicitly supposed there that the account of the interrelation between ε and γ can lead only to insignificant modifications of the phase diagrams withoug changing qualitative conclusions. Catastrophe theory allows us to substantiate that such a point of view is not correct and to solve the problem adequately and completely in terms of a

topological analysis. If we analyse figures 14 and 15 from the point of view of catastrophe theory then it becomes clear that curves being sections of physical critical manifolds of our model in corresponding coordinates are shown in these figures. It should be recalled that physical and mathematical critical manifolds differ by the fact that the former are given by equations (12) together with the equilibrium conditions (i.e. by equalities of free energies of the different phases) and the latter are determined by the same equations but combined with the stability conditions (18). Here only physical critical manifolds are considered. Their three dimensional pictures reconstructed according to the corresponding plane sections (see figures 14 and 15) are shown in figures 16–19 (*a*) and (*b*) in coordinates $(\varepsilon, \gamma, \langle P_2 \rangle)$ and (ε, γ, x), respectively. We note that the characteristic form of the critical manifolds as surfaces of the fold type is due to the realization of the swallowtail catastrophe in the model [13, 14].

Without performing numerical calculations it follows from figure 2 that there are four fundamentally different versions of the behaviour of monotonically decreasing functions $\varepsilon(\gamma)$ which are determined by the location of the curves with respect to the boundaries between areas I–IV in the plane of the variables ε–γ: (1) the curve $\varepsilon(\gamma)$ does not intersect the boundaries of areas I–IV (see figure 16), (2) the curve $\varepsilon(\gamma)$ crosses all the boundaries (see figure 17), (3) it enters area III from the side of area II crossing boundaries between areas I and II, II and III (see figure (18), (4) the curve $\varepsilon(\gamma)$ enters area III on the side from area IV crossing the boundary between areas III and IV (see figure 19). In figures 16–19 in the three dimensional coordinate systems $(\varepsilon, \gamma, \langle P_2 \rangle)$, (ε, γ, t) cylindrical surfaces with guides given functionally $\varepsilon = \varepsilon(\gamma)$ correspond to these curves. Hence, it follows immediately that for four cases described the two dimensional phase diagrams of the model and the dependences of the critical values of the orientational

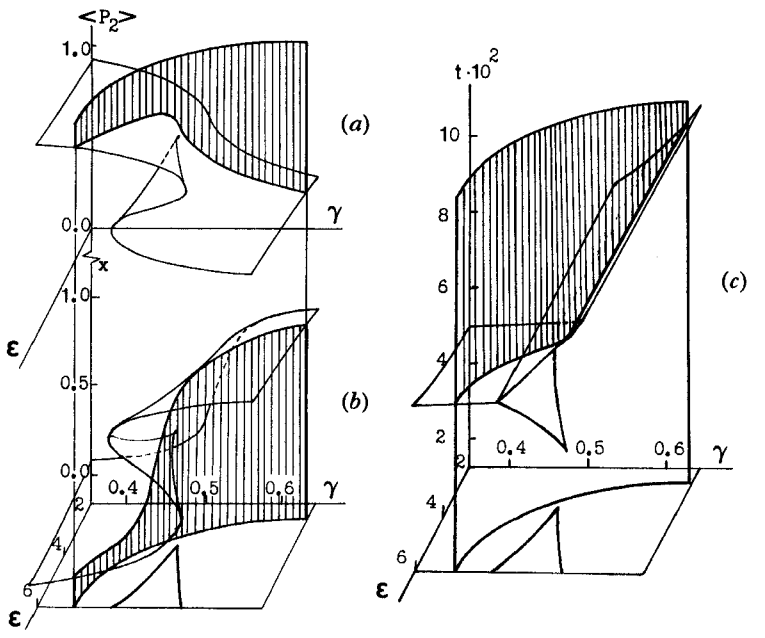

Figure 16. Critical values of the orientational order (*a*) and conformational disorder (*b*) parameters and phase diagram (*c*) of our model in cylindrical coordinates for the first characteristic version of the dependence $\varepsilon(\gamma)$.

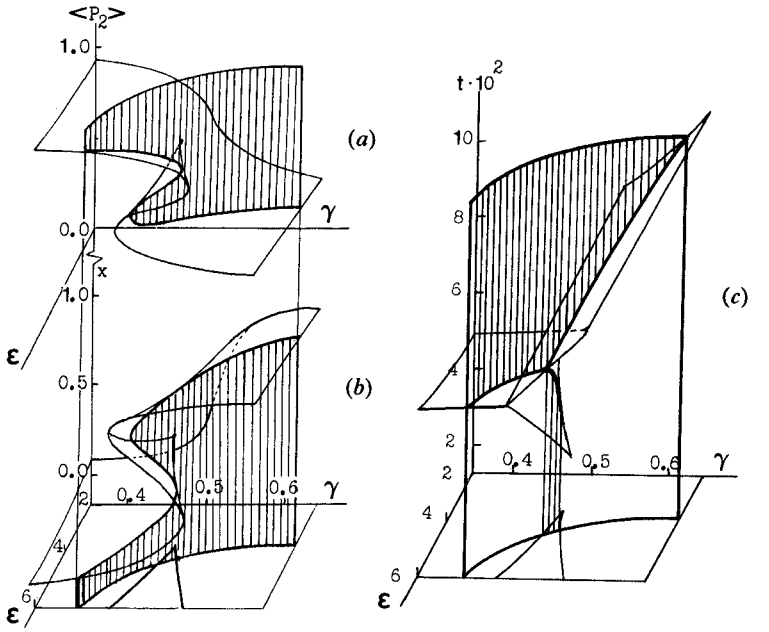

Figure 17. Critical values of the orientational order (*a*) and conformational disorder (*b*) parameters and phase diagram (*c*) of our model in cylindrical coordinates for the second characteristic version of the dependence $\varepsilon(\gamma)$.

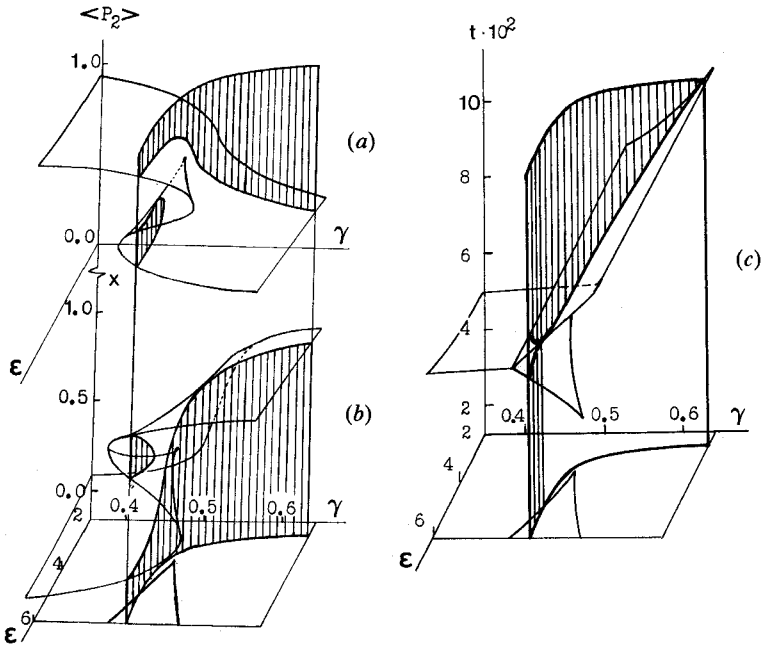

Figure 18. Critical values of the orientational order (*a*) and conformational disorder (*b*) parameters and phase diagram (*c*) of our model in cylindrical coordinates for the third characteristic version of the dependence $\varepsilon(\gamma)$.

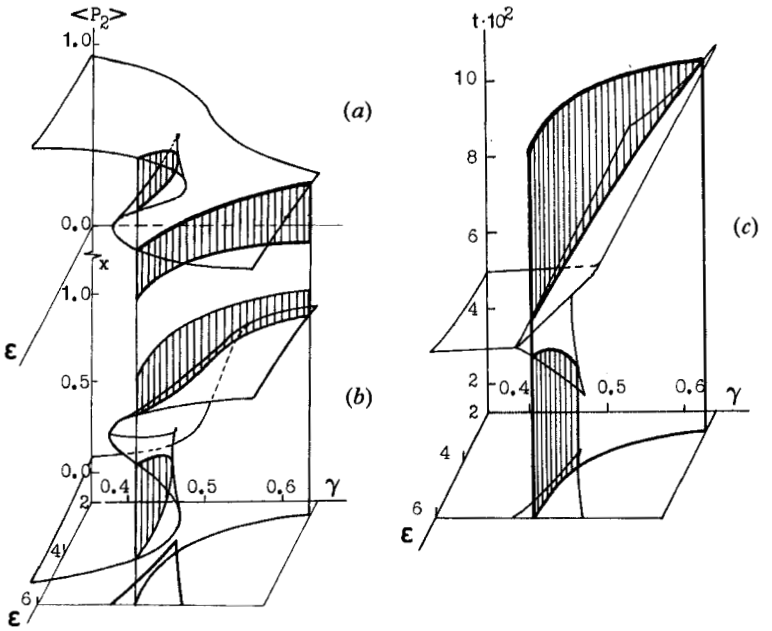

Figure 19. Critical values of the orientational order (*a*) and conformational disorder (*b*) parameters and phase diagram (*c*) of our model in cylindrical coordinates for the fourth characteristic version of the dependence $\varepsilon(\gamma)$.

order and conformational disorder parameters on the length and flexibility of particles are realized in corresponding cylindrical sections of the Maxwell set (see figures 16 (*c*)–19 (*c*)) and critical manifolds $\langle P_2 \rangle(\varepsilon, \gamma)$ (see figures 16 (*a*)–(19 (*a*)) and $x(\varepsilon, \gamma)$ (see figures 16 (*b*)–19 (*b*)). It follows from comparison of figures 16–19 and 4–6, 14 and 15 that the topology of the curves in cylindrical coordinates is equivalent to that of the corresponding curves in orthogonal plane coordinates. Therefore, all of the qualitative conclusions about the phase diagrams of the model (see figures 3–6) and the behaviour of the critical order parameters (see figures 14 and 15) remain valid but the following circumstances should be kept in mind: they belong to certain types of the dependences $\varepsilon(\gamma)$ (see figures 16 (*b*)–19 (*b*)). Two conclusions follow from this.

First, taking into account that there should be specific interconnections between the molecular length and flexibility in homologous series of mesogenic compounds, in a number of cases homologous series of even very similar compounds (close dependences for $\varepsilon(\gamma)$) can essentially differ by critical parameters (cf. figures 16 (*a*) and (*b*)–19 (*a*) and (*b*)) and be characterized by topologically different phase diagrams (for example, in temperature–number of carbon atoms in aliphatic tails of particles coordinates) (see figures 16 (*c*)–19 (*c*). Similar effects relevant to transitions of the plastic crystal–liquid crystal type take place, for example, for different metal ions in chlorine-metalalkylammonium compounds [42]. In this aspect, steric effects of substituents in conjugated mesogens which lead to an essential modification of the phase diagrams including the formation of intermediate phases are of interest in liquid crystal research [43].

The second conclusion bears a relation to [18] in which a $\varepsilon(\gamma)$ dependence corresponding to figure 17 is considered and the results are interpreted in accord with graphic information similar to that shown in figure 15 which is, apparently, not correct

(cf. figures 17 (*a*) and (*b*) and 15). As a consequence, for example, the terminal critical point was not found in [19] which is really absent in the phase diagrams of figures 6, 18 (*c*) and 19 (*c*) but is available in the phase diagrams shown in figures 17 and 19. In this connection the experimental paper [44] attracts attention in which a line of isostructural transformations quasibilayer–bilayer smectic terminating in a critical point similar to that found in the phase diagrams of figures 5 and 17 (*c*) occurs in the temperature–concentration plane for mixtures of cyano compounds. It is to be taken into account here that a change of the molecular flexibility corresponds to that of the relative concentration of the components. This substantiates a supposition that for the cyano compounds studied in [44] the translational order of the smectic phase contributes mainly to the formation of the optimum combination of the particles flexibility and orientational order of the system and the isostructural transition between quasibilayer–bilayer states, by analogy to our results, is induced by conformational disordering of the aromatic fragments of molecular dimers paired by means of the interaction of oppositely directed dipoles of the cyano groups. We also note a theoretical paper [45] in which a phase diagram with the critical end point in the line between nematic phases of comb shaped liquid-crystalline polymers is built. In this case a corresponding isostructural transformation can be intepreted only from the point of view of the conformations of the main chain and flexible spacers by which mesogenic fragments are attached to it.

6. Conclusion

Catastrophe theory provides a perspective trend in the study of molecular gradient systems stability which determines a strategy for solving multiparametric physical problems. Catastrophe theory has usually been used in physical developments for illustrative purposes only and a consideration has been fulfilled using examples of the canonic one parametric, lowest order catastrophes taken from Thom's famous table [14]. In addition, catastrophe theory calculations are, in their meaning, close to the phenomenologic (Landau) descriptions, which is certainly important in itself but does not give a possibility of their direct use in statistical thermodynamics. Our paper is an attempt to apply catastrophe theory to the study of non-trivial thermodynamic potentials in statistical mechanical problems involving liquid crystals. We attempt now to underline some results bound up with the mathematical aspects of the methods applied.

(i) It is shown that not one but a greater number of catastrophes (in our case these are the fold and swallowtail ones) can arise in a physical model which leads to the non-standard separatix structure (see figures 1–3) and, hence, to non-standard phase diagrams (see figures 2–6).

(ii) A catastrophe with a non-universal unfolding appears to be a physically significant one. This one is a fold in the case under consideration and, moreover, the non-universal perturbation (unlike the universal one described by Thom's table of elementary catastrophes [13]) does not lead to a potential topology change on passing through a specific point but determines a thermodynamic stability type of the most symmetric (isotropic liquid) state (see [14] and figures 3–6).

(iii) Not each of the catastrophes separately but their interaction (or superposition) in control parameter space determines the themodynamic potential topology and, hence, the behaviour of the system. In the case considered this merely

means that all of the qualitative results of our model can be obtained on the basis of the investigation of two simple polynomials (29) and (44). While constructing the free energy graphs (see figures 3–13), graphs of these polynomials should be combined in such a manner that the topology of the potentials of the fold and swallowtail catastrophes is preserved.

(iv) In connection with a previous result we emphasize one more non-trivial circumstance bound up with the ideology of a popular theory of phase transitions, namely the Landau description which is a particular case of catastrophe theory. The Landau theory based on the expansion of the free energy in a power series of order parameter proceeds from the cusp catastrophe in the simplest case. In addition, the fold and swallowtail catastrophes are excluded from consideration of the Landau theory on the ground that they either do not allow us to model a positive equilibrium order parameter value of a low symmetry phase or do not describe correctly the stability conditions of a high symmetry phase. However, as we have shown, though each of the catastrophes apart leads to the non-physical topology of the thermodynamic potential, in contrast, their superposition in the control parameter space does determine a physically reasonable topology of the potential. (In this context a physically reasonable topology of the potential means the following asymptotic behaviour: $\Psi(x) \Rightarrow +\infty$ at $\|x\| \Rightarrow \infty$, where x is a multidimensional order parameter.) It can be supposed that a superposition of catastrophes is a typical situation in complex statistical mechanical models; however, from the viewpoint of Landau theory it has never been explicitly considered earlier, though, apparently, it could broaden the range of physically significant phenomenological models.

Appendix I

In this Appendix formulae for coefficients b_{ij} of the Taylor series (34) are presented.

$$\left.\begin{aligned} b_{01} &= \langle P_2\rangle_0'[2/3a^0 t - \langle P_2\rangle_0 Q^2(x^0,\gamma)], \\ b_{10} &= t\ln[x^0/(1-x^0)] - t\varepsilon - \langle P_2\rangle_0^2(1-\gamma)Q(x^0,\gamma), \end{aligned}\right\} \tag{A 1}$$

$$\left.\begin{aligned} b_{02} &= \langle P_2\rangle_0''[1/3a^0 t - 1/2\langle P_2\rangle_0 Q^2(x^0,\gamma)] + \langle P_2\rangle_0'[1/3t - 1/2\langle P_2\rangle_0' Q^2(x^0,\gamma)], \\ b_{11} &= -2\langle P_2\rangle_0\langle P_2\rangle_0' Q(x^0,\gamma)(1-\gamma), \\ b_{20} &= 1/2[t/[x^0(1-x^0)] - \langle P_2\rangle_0^2(1-\gamma)^2], \end{aligned}\right\} \tag{A 2}$$

$$\left.\begin{aligned} b_{03} &= 1/9t[2\langle P_2\rangle_0'' + a^0\langle P_2\rangle_0^{(3)}] - 1/2[\langle P_2\rangle_0'\langle P_2\rangle_0'' + 1/3\langle P_2\rangle\langle P_2\rangle_0^{(3)}]Q^2(x^0,\gamma), \\ b_{12} &= -[\langle P_2\rangle_0\langle P_2\rangle_0'' + \langle P_2\rangle_0'^2]Q(x^0,\gamma)(1-\gamma), \\ b_{21} &= -\langle P_2\rangle_0\langle P_2\rangle_0'(1-\gamma)^2, \\ b_{30} &= t(2x^0-1)/[6(x^0)^2(1-x^0)^2], \end{aligned}\right\} \tag{A 3}$$

$$\left.\begin{aligned} b_{04} &= 1/36t[3\langle P_2\rangle_0^{(3)} + a^0\langle P_2\rangle_0^{(4)}] - 1/6[\langle P_2\rangle_0'\langle P_2\rangle_0^{(3)} \\ &\quad + 1/4\langle P_2\rangle_0\langle P_2\rangle_0^{(4)}]Q^2(x^0,\gamma), \\ b_{13} &= -[\langle P_2\rangle_0'\langle P_2\rangle_0'' + 1/3\langle P_2\rangle_0\langle P_2\rangle_0^{(3)}]Q(x^0,\gamma)(1-\gamma), \\ b_{22} &= -1/2[\langle P_2\rangle_0\langle P_2\rangle_0'' + \langle P_2\rangle_0'\langle P_2\rangle_0'](1-\gamma)^2, \quad b_{31} = 0, \\ b_{40} &= t[3(x^0)^2 - 3x^0 + 1]/[12(x^0)^3(1-x^0)^3], \end{aligned}\right\} \tag{A 4}$$

$$\left.\begin{aligned}
b_{05} &= -1/12[\langle P_2\rangle_0''\langle P_2\rangle_0^{(3)} + 1/2\langle P_2\rangle_0'\langle P_2\rangle_0^{(4)} + 1/10\langle P_2\rangle_0\langle P_2\rangle_0^{(5)}]Q^2(x^0,\gamma)\\
b_{14} &= -1/3[\langle P_2\rangle_0\langle P_2\rangle_0^{(3)} + 1/4\langle P_2\rangle_0\langle P_2\rangle_0^{(4)}]Q(x^0,\gamma)(1-\gamma),\\
b_{23} &= -1/2[\langle P_2\rangle_0\langle P_2\rangle_0'' + 1/3\langle P_2\rangle_0\langle P_2\rangle_0^{(3)}](1-\gamma),\\
b_{32} &= 0, \quad b_{41} = 0,\\
b_{50} &= 1/20t[(x^0)^4 - (1-x^0)^4]/[(x^0)^4(1-x^0)^4].
\end{aligned}\right\} \quad \text{(A 5)}$$

In equations (A 1)–(A 5) $\langle P_2\rangle_0'$, $\langle P_2\rangle_0''$, …, $\langle P_2\rangle_0^{(5)}$ are derivatives of the orientational order parameter from equation (13) with respect to variable a up to fifth order inclusive at the account of equation (14) in the point $a=a^0\neq 0$. In the numerical analysis of the problem, it is convenient to use equations expressing these derivatives through the quantity a (see equation (13)) and the order parameter. From equations (13) and (14) we find

$$\langle P_2\rangle^{(i)} = \sum_{j=0}^{i+1} h_{ij}\langle P_2\rangle^j, \quad i=1,\ldots,5. \qquad \text{(A 6)}$$

where h_{ij} are

$$\left.\begin{aligned}
h_{10} &= 1/3,\\
h_{11} &= 1/3 - 3/(2a),\\
h_{12} &= -2/3,
\end{aligned}\right\} \quad \text{(A 7)}$$

$$\left.\begin{aligned}
h_{20} &= 1/9 - 1/(2a),\\
h_{21} &= -1/3 - 1/a + 15/(4a^2),\\
h_{22} &= -2/3 + 3/a,\\
h_{23} &= 8/9,
\end{aligned}\right\} \quad \text{(A 8)}$$

$$\left.\begin{aligned}
h_{30} &= -1/9 - 1/(3a) + 7/(4a^2),\\
h_{31} &= -5/9 + 13/(6a) + 15/(4a^2) - 105/(8a^3),\\
h_{32} &= 2/3 + 14/(3a) - 11/a^2,\\
h_{33} &= 16/9 - 8/a.\\
h_{34} &= 16/9,
\end{aligned}\right\} \quad \text{(A 9)}$$

$$\left.\begin{aligned}
h_{40} &= 5/27 + 13/(18a) + 19/(12a^2) - 63/(8a^3),\\
h_{41} &= -7/27 + 14/(3a) - 23/(2a^2) - 35/(2a^3) + 945/(16a^4),\\
h_{42} &= 70/27 - 25/(3a) - 57/(2a^2) + 255/(4a^3),\\
h_{43} &= -40/27 - 200/(9a) + 176/(3a^3),\\
h_{44} &= 160/27 + 80/(3a),\\
h_{45} &= 128/27,
\end{aligned}\right\} \quad \text{(A 10)}$$

$$\left.\begin{aligned}
h_{50} &= -7/81+14/(9a)-41/(9a^2)-9/a^3+693/(16a^4),\\
h_{51} &= 147/81-79/(18a)-207/(6a^2)+923/(12a^3)+1575/(16a^4)-10395/(32a^5),\\
h_{52} &= 2/27-119/(3a)+242/(3a^2)+838/(6a^3)-3375/(8a^4),\\
h_{53} &= -1040/81+280/(9a)+1970/(9a^2)-1399/(3a^3),\\
h_{54} &= 80/27+1040/(9a)-304/a^2,\\
h_{55} &= 640/27-960/(9a),\\
h_{56} &= -1280/81.
\end{aligned}\right\} \quad \text{(A 11)}$$

Appendix II

In this Appendix formulae for the coefficients c_{ij} in the potential representation (40) are calculated

$$\beta_{01} = b_{10}b_{11} - b_{01}G, \quad \text{(A 12)}$$

$$\alpha = b_{10}G + b_{01}b_{11}, \quad \text{(A 13)}$$

$$\delta = \lambda_1(G^2 + b_{11}^2), \quad \text{(A 14)}$$

$$\mu = \lambda_2(G^2 + b_{11}^2), \quad \text{(A 15)}$$

$$\left.\begin{aligned}
c_{03} &= -b_{03}G^3 + b_{11}b_{12}G^2 - b_{21}b_{11}^2G + b_{30}b_{11}^3,\\
c_{12} &= b_{12}G^3 + b_{11}(3b_{03} - 2b_{21})G^2 + b_{11}^2(3b_{30} - 2b_{12})G + b_{21}b_{11}^3,\\
c_{21} &= -b_{21}G^3 + b_{11}(3b_{30} - 2b_{12})G^2 + b_{11}^2(2b_{21} - 3b_{03})G + b_{12}b_{11}^3,\\
c_{30} &= b_{30}G^3 + b_{11}b_{21}G^2 + b_{12}b_{11}^2G + b_{03}b_{11}^3,
\end{aligned}\right\} \quad \text{(A 16)}$$

$$\left.\begin{aligned}
c_{04} &= b_{04}G^4 - b_{11}b_{13}G^3 + b_{22}b_{11}^2G^2 + b_{40}b_{11}^4,\\
c_{13} &= -b_{13}G^4 + 2b_{11}(b_{22} - 2b_{04})G^3 + 3b_{13}b_{11}^2\Gamma^2 + 2b_{11}^3G(2b_{40} - b_{22}),\\
c_{22} &= b_{22}G^4 + 3b_{11}b_{13}G^3 + 2b_{11}^2(3b_{04} - 2b_{22} + 3b_{40})G^2 - 3b_{13}b_{11}^3G,\\
c_{31} &= 2b_{11}(2b_{40} - b_{22})G^3 - 3b_{11}^2b_{13}G^2 + 2b_{11}^3(b_{22} - 2b_{04})G + b_{13}b_{11}^4,\\
c_{40} &= b_{40}G^4 + b_{11}^2b_{22}G^2 + b_{11}^3b_{13}G + b_{04}b_{11}^4,
\end{aligned}\right\} \quad \text{(A 17)}$$

$$\left.\begin{aligned}
c_{05} &= -b_{05}G^5 + b_{11}b_{14}G^4 - b_{23}b_{11}^2G^3 + b_{50}b_{11}^5,\\
c_{14} &= b_{14}G^5 + b_{11}(5b_{05} - 2b_{23})G^4 - 4b_{14}b_{11}^2G^3 + 3b_{11}^3b_{23}G^2 + 5b_{11}^4b_{50}G,\\
c_{23} &= -b_{23}G^5 - 4b_{11}b_{14}G^4 + 2b_{11}^2(3b_{23} - 5b_{05})G^3\\
&\quad + 2b_{11}^3(5b_{50} + 3b_{14})G^2 - 3b_{23}b_{11}^4G,\\
c_{32} &= 2b_{11}^2(5b_{50} + 3b_{14})G^3 + 3b_{11}b_{23}G^4 + 2b_{11}^3(5b_{05} - 3b_{23})G^2\\
&\quad + b_{23}b_{11}^5 - 4b_{11}^4b_{14}G,\\
c_{41} &= 5b_{50}b_{11}G^4 - 3b_{23}b_{11}^2G^3 - 4b_{14}b_{11}^3G^2 + b_{11}^4(2b_{23} - 5b_{50})G + b_{14}b_{11}^5,\\
c_{50} &= b_{50}G^5 + b_{11}^3b_{23}G^2 + b_{11}^4b_{14}G + b_{05}b_{11}^5.
\end{aligned}\right\} \quad \text{(A 18)}$$

Appendix III

We calculate the coefficients in equations (45) with the help of perturbation theory for the coefficient α (see equation (A 13)) being infinitely small in the limit $(\varepsilon,\gamma,t)\to(\varepsilon^0,\gamma^0,t^0)$. According to [14, 15] it is sufficient to find the coefficients λ, A, B, F, D of the polynomial (45) in first order of perturbation theory over α and the coefficient E in (45) and the coefficients of the transformation (44) in zeroth order. In addition, all of the topological features of the potential (11) are retained, at least locally in the neighbourhood of the transition (42). As a result we have

$$\left.\begin{aligned}
&\lambda\approx\lambda^0+\alpha\lambda^1=\mu-\alpha A^0_{20},\quad A\approx A^0+\alpha A^1=\beta_{01}+\alpha b^0,\\
&B\approx B^0+\alpha B^1=\delta-\alpha A^0_{02},\quad F\approx F^0+\alpha F^1=c_{03}+\alpha(A^0_{02}A^0_{11}-A^0_{03},\\
&D\approx D^0+\alpha D^1=(4\mu c_{04}-c_{12}^2)/(4\mu)\\
&\quad+\alpha[-A^0_{04}+A^0_{11}A^0_{03}+A^0_{02}A^0_{12}-A^0_{20}(A^0_{02})^2\ -A^0_{20}(A^0_{11})^2],\\
&E\approx E^0=1/(4\mu^2)[4\mu^2c_{05}-2\mu c_{12}c_{13}+c_{21}c_{12}^2],
\end{aligned}\right\}\tag{A 19}$$

$$A_{ij}\approx A^0_{ij},\quad A^0_{02}=c_{12}/(2\mu),$$

$$A^0_{11}=c_{21}/(2\mu),\quad A^0_{20}=c_{30}/(2\mu),\tag{A 20}$$

$$\left.\begin{aligned}
&A^0_{03}=1/(4\mu^2)[2\mu c_{13}-c_{21}c_{12}],\quad A^0_{12}=1/(8\mu^2)[4\mu c_{22}-c_{21}^2-2c_{30}c_{12}],\\
&A^0_{21}=1/(4\mu^2)[2\mu c_{31}-c_{21}c_{30}],\quad A^0_{30}=1/(8\mu^2)[4\mu c_{40}-c_{30}^2],\ldots.
\end{aligned}\right\}\tag{A 21}$$

$$e\approx e^0+\alpha e^1=-\alpha A_{11}/(2\mu).\tag{A 22}$$

In equations (A 19)–(A 22) the superscripts 0 and 1 correspond to zeroth and first orders of their expansions relative to α.

References

[1] CHANDRASEKHAR, S., 1977, *Liquid Crystals* (Cambridge University Press).
[2] AVERYANOV, E. M., 1987, *Liq. Crystals*, **2**, 491.
[3] MARCELJA, S., 1974, *J. chem. Phys.*, **60**, 3599.
[4] EMSLEY, J. W., and LUCKHURST, G. R., 1980, *Molec. Phys.*, **41**, 19.
[5] EMSLEY, J. W., LUCKHURST, G. R., and STOCKLEY, C. P., 1982, *Proc. R. Soc.* A, **381**, 117.
[6] COUNSELL, C. J. R., EMSLEY, J. W., HEATON, N., and LUCKHURST, G. R., 1985, *Molec. Phys.*, **54**, 847.
[7] EMSLEY, J. W., HASHIM, R., LUCKHURST, G. R., and SHILSTONE, G. N., 1986, *Liq. Crystals*, **1**, 437.
[8] LUCKHURST, G. R., 1988, *J. chem. Soc. Faraday Trans. 2*, **84**, 961.
[9] RONCA, G., and YOON, D. Y., 1982, *J. chem. Phys.*, **76**, 3295.
[10] SIGAUD, G., YOON, D. Y., and GRIFFIN, A. C., 1983, *Macromolecules*, **16**, 375.
[11] YOON, D.Y., BRUCKNER, S., VOLKSEN, W., SCOTT, J. C., and GRIFFIN, A. C., 1985, *Faraday Discuss. chem. Soc.*, **79**, 41.
[12] THOM, R., 1972, *Stabilité Structurelle et Morphogenese* (Benjamin).
[13] POSTON, T., and STEWART, I., 1978, *Catastrophe Theory and its Applications* (Pitman).
[14] GILMORE, R., 1981, *Catastrophe Theory for Scientists and Engineers* (Interscience).
[15] ARNOLD, V. I., 1983, *Catastrophe Theory* (Moscow University).
[16] CAILLE, A., PINK, D., VERTENIL, F., and ZUCKERMANN, M. J., 1980, *Can. J. Phys.*, **58**, 581.
[17] KIMURA, H., and NAKANO, H., 1977, *J. phys. Soc. Japan*, **43**, 1477.
[18] KIMURA, H., and NAKANO, H., 1979, *J. phys. Soc. Japan*, **46**, 1695.
[19] KIMURA, H., and NAKANO, H., 1981, *Molec. Crystals liq. Crystals*, **68**, 289.
[20] PINK, D. A., *Can. J. biochem. Biol.*, **62**, 760.
[21] LEGRE, J. P., FIPRO, J. L., and ALBINET, G., 1985, *Phys. Rev.* A, **31**, 1703.

[22] KONOPLEV, V. A., and PERSHIN, VL. K., 1987, *Khim. Phys.*, **6**, 855.
[23] KONOPLEV, V. A., and PERSHIN, VL. K., 1988, *Khim. Phys.*, **7**, 425.
[24] FEYNMAN, R. P., 1972, *Statistical Mechanics* (Benjamin).
[25] PERSHIN, V. K., and PERSHIN, VL. K., 1986, *Zh. Phys. Khim.*, **60**, 300.
[26] BLUMSTEIN, R. B., STICKLES, E., and BLUMSTEIN, A., 1982, *Molec. Crystals liq. Crystals*, **82**, 205.
[27] BLUMSTEIN, A., BLUMSTEIN, R. B., GAUTHIER, M. M., THOMAS, O., and ASRAR, J., 1983, *Molec. Crystals liq. Crystals*, **92**, 87.
[28] MAIER, W., and SAUPE, A., 1959, *Z. Naturf.* (*a*), **13**, 564.
[29] PERSHIN, VL. K., and KONOPLEV, V. A., 1990, *Solid State Commun.*, **76**, 1131.
[30] MELY, B., and CHAVROLIN, J., 1977, *Chem. Phys. Lipids*, **19**, 43.
[31] HUBBELL, W. L., and MCCONNELL, H. M., 1971, *J. Am. chem. Soc.*, **94**, 314.
[32] KRISHNAMURTI, O., and SOMASEKHAR, R., 1981, *Molec. Crystals liq. Crystals*, **75**, 133.
[33] DUNMUR, D. A., and WILSON, M. R., 1988, *J. chem. Soc. Faraday Trans. 2*, **84**, 1109.
[34] FINKELMANN, H., BENTHACK, H., and REHAGE, G., 1983, *J. Chim. phys.*, **80**, 163.
[35] CHUVIROV, A. N., 1974, *Kristallographiya*, **19**, 297.
[36] SIMOVA, P., and PETROV, M., 1981, *J. Phys.* D, **14**, 1.
[37] SIMOVA, P., PETROV, M., and NIKOLOVA, E., 1982, *Acad. bulg. Sci.*, **35**, 1371.
[38] BLUMSTEIN, A., VILASAGAR, S., PONRATHNAM, S., CLOUGH, S., MARET, G., and BLUMSTEIN, R. B., 1983, *J. Polym. Sci. Polym. Sci. Ed.*, **20**, 877.
[39] MARTINS, A., FERREIRA, J., VOLINO, F., BLUMSTEIN, A., and BLUMSTEIN, R. B., 1983, *Macromolecules*, **16**, 279.
[40] FURUYA, K., and MITSUI, T., 1979, *J. phys. Soc. Japan*, **46**, 611.
[41] TANAKA, H., and FREED, J. H., 1984, *J. phys. Chem.*, **88**, 6633.
[42] BLINC, R., KOZELJ, M., RUTAR, V., ZUPANICIC, I., and ZEKS, B., 1980, *Faraday Discuss. chem. Soc.*, **69**, 58.
[43] SADASHIVA, B., 1984, *Molec. Crystals liq Crystals*, **110**, 309.
[44] SHADIDHAR, R., RATNA, B., PRASAD, S., and SOMASEKHARA, S., 1987, *Phys. Rev. Lett.*, **59**, 1209.
[45] RENZ, W., and WARNER, M., 1988, *Proc. R. Soc.* A, **417**, 213.